Numerical methods for coupling multigroup radiation with ion and electron temperatures.

C. Enaux[1], S. Guisset[2], C. Lasuen, G. Samba

Abstract. This paper is devoted to the numerical approximation of a multigroup three temperature plasma model. A reformulation of the model is proposed in order to derive robust convex combination-based schemes. The produced schemes are naturally well-suited to handle stiff source terms and can be analyzed. However, because of the very large size of the resulting linear system, a direct numerical solving can not be performed in practice if a large number of cells or frequency groups is used. Consequently, a decoupling procedure is presented in order to greatly reduce the numerical cost of the method while keeping the fundamental discrete properties. After detailing the schemes derivation followed by the practical numerical resolution and the decoupling procedure, a numerical analysis is performed, and strong stability properties are proven. Several numerical test cases are carried out to demonstrate the interest of the numerical approach.

Key words. multigroup three temperature model, numerical schemes, plasma physics, radiative transfer

Introduction

Background.
From stars dynamics to Inertial Confinement Fusion, it is well-known that radiative transport coupled with plasma physics hydrodynamics plays a key role in such complex processes. However, full three-dimensional frequency-dependent transport-based direct simulations are still too expensive for most computer architectures. Over the years, various reduced physical models have been proposed to address this issue. In general the dimension of the problem studied is reduced in order to significantly decrease the numerical costs while keeping the main features of the underlying equations model of radiative transfer. While reduced models enables to greatly reduce the computational cost they are often integrated with respect to the frequency variable (grey approximation) since frequency-dependent descriptions are generally not affordable. However, in various astrophysical applications (such as star formations for example [13, 14]) the frequency-dependence of the opacities (inside the interstellar gas) must be correctly taken into

[1]CEA-DIF, France. E-mail: cedric.enaux@cea.fr
[2]CEA-DIF, France. E-mail: sebastien.guisset@cea.fr

account [11, 23]. In this field it is observed that the frequency-dependence is particularly sensitive. Consequently, one understands here the difficulty encountered when dealing with large frequency-variation problems.

Multigroup approaches have emerged to perform frequency dependent simulations [5, 27, 30]. In this case the frequency variable is sampled into a finite number of groups and the frequency integration is only performed over the groups. The main advantage of multigroup methods comes from the fact that with a relatively small number of groups strong opacity variation may be considered. Of course, this suppose an efficient and sufficient frequency-resolution where it is required. In general the frequency-group distribution is carefully set at the beginning of the simulation. We mention here that adaptive frequency domain strategies have been studied in [28, 7]. Various one dimension neutrino radiation simulation code have been developed over the years, see for example [2, 3, 17]. Concerning the development of grey diffusion code we refer to the large literature on the subject [20, 8] and the references therein. Two dimension multigroup codes have been developed more recently [**?**, 25, 30, 12] but the scientific literature on the subject remains relatively low and the development of robust discretizations is still a challenging issue. Among the most advanced works we mention [25] and the related work [30] where the 2D multigroup model used is obtained using the comoving-frame approach so it is correct up to the order $O(v/c)$ (where v is a characteristic velocity of the problem and c the speed of light). We also mention the work [12] in which a standard direct time implicit solver using a stabilized bi-conjugate algorithm is used and thanks to a mesh refinement strategies first three dimension simulations were carried out.

In addition to correctly model the photon transport to take into account stiff radiative effects, the modeling of charged particles is also required in most astrophysics [10] or inertial confinement fusion [7] applications. On this topic, the relaxation time between the electronic and ionic temperatures toward the same temperature occurs on a time scale much larger than the ones required to reach quasi-neutral regimes or required for the electron and ion distribution functions to reach Maxwellian equilibrium distributions [6]. However, the characteristic times of interest can be of the same order of the temperature relaxation times. When this is the case, two-temperature hydrodynamics models have to be considered [6]. In the present work the multigroup radiation equations are then coupled with energy evolution equations for electrons and ions.

Present approach, aim and outline.
While the numerical cost involved when working with multigroup radiation-hydrodynamics models still remains problematic (despite the large efforts recently undertaken as mentioned in the former paragraph), we also point out that the numerical analysis side of the developed method remains largely unexplored. Indeed, because of the non-linearity of the models coupled with the stiffness of the equations, time implicit solvers based on standard linearisation strategies are very often used. However, we emphasize that a numerical resolution based on a direct Newton-Raphson-type strategy does not ensure that the numerical solution remains positive at each sub-iteration and may lead to divergence issues. Some numerical analysis elements can be found in [21, 15, 1] however

in most of the works, despite an extensive numerical validation with various numerical experiments, no numerical analysis of the schemes is carried out. In particular the issue of the stability of the method, the preservation of the positivity of the discrete solutions nor the convergence of the method is really addressed.

In this context, the present work does not intend to simply presents another multigroup radiation-hydrodynamics code. The aim consists in providing a robust numerical approach which is suitable for a numerical analysis. To achieve this, the ideas introduced in [8] for a grey three temperature model are now extended to this multigroup context. This strategy is based on a reformulation of the model and allows to prove some interesting numerical properties such as unconditional stability, convergence, energy conservation and asymptotic preservation. A reformulation of the three temperature multigroup model studied here is performed in order to derive robust convex combination-based schemes. The resulting schemes are naturally well-suited to handle stiff source terms and can be analyzed. However, because of the very large size of the resulting linear system, a direct numerical solving can not be performed in practise if a large number of cells or frequency groups is used. Consequently, a decoupling procedure is presented in order to greatly reduce the numerical cost of the method while keeping the fundamental discrete properties. The difficulties encountered and the solutions proposed are clearly explained in the present document.

This work is organized as follows. Firstly, we present the three temperature multigroup model and its associated reformulation. Hence the numerical strategy adopted is detailed and a numerical analysis of the scheme is presented. Secondly, the methodology is extended to the one dimensional setting to include the contribution of the radiative flux. The numerical analysis is extended accordingly. Thirdly, the numerical strategy studied is validated with various numerical experiments. Finally, our conclusions and perspectives are given.

1 Model derivation

1.1 Spectral equation

In this section, the model studied and its derivation are briefly presented. We start this derivation by the LTE version of the transport equation, where we assume the source function is Planckian in accordance with the Kirchhoff-Planck relation. It describes the absorption and emission phenomena of the photons when crossing matter at rest (no hydrodynamics) [19]

$$\frac{1}{c}\frac{\partial I_\nu}{\partial t} + \omega \cdot \nabla I_\nu + \sigma_\nu I_\nu = \sigma_\nu B_\nu, \tag{1}$$

where $I_\nu(t, x, \omega, \nu)$ denotes the radiative intensity (also called the spectral intensity) for photons located in x with frequency ν and whose direction is ω. The quantity $I_\nu(t, x, \omega, \nu)$ can be linked to the photons density N located at x with frequency ν and with direction ω by the relation $I_\nu(t, x, \omega, \nu) = ch\nu N(t, x, \omega, \nu)$. The speed of light is c and the Planck constant is h. The opacity of the matter with an electronic temperature

T_e for a radiation of frequency ν is denoted $\sigma_\nu(\nu, T_e)$ while the radiative intensity of a black body is written B_ν. Finally the Planck distribution $B_\nu(\nu, T_e)$ is defined by

$$B_\nu(\nu, T_e) = b_\nu(\nu, T_e)\frac{c}{4\pi}\phi_e, \qquad \phi_e = aT_e^4,$$

where the radiative constant a and the reduced Planck distribution b_ν read

$$a = \frac{8\pi^5 k^4}{15c^3h^3}, \qquad b_\nu(\nu, T) = \frac{15h^4\nu^3}{\pi^4 k_b^4 T_e^4}\frac{1}{\exp(\frac{h\nu}{k_b T}) - 1}, \qquad \int_0^{+\infty} b_\nu(\nu, T_e)d\nu = 1.$$

1.2 Multigroup equations

Define G groups (*ie* intervals of the form $[\nu_{g-1}, \nu_g[)$ which form a partition of $\mathbb{R}^+$. By integrating (1) over the group g (in other words, over the interval $[\nu_{g-1}, \nu_g[)$ leads formally to

$$\frac{1}{c}\frac{\partial I_g}{\partial t} + \omega \cdot \nabla I_g + \sigma_g^{abs} I_g = \frac{c}{4\pi}\sigma_g^{em} b_g \phi_e, \qquad \text{for } \ g \in \{1; 2; ...; G\}, \tag{2}$$

with

$$I_g = \int_{\nu_{g-1}}^{\nu_g} I_\nu d\nu, \qquad \sigma_g^{abs} = \frac{1}{I_g(t, x, \omega)}\int_{\nu_{g-1}}^{\nu_g} \sigma_\nu(\nu, T_e) I_\nu(t, x, \omega, \nu)d\nu,$$

and the Planck means per group

$$\sigma_g^{em} = \sigma_g(T_e) = \frac{1}{b_g(T_e)}\int_{\nu_{g-1}}^{\nu_g} \sigma_\nu(\nu, T_e) b_\nu(\nu, T_e)d\nu,$$

where

$$b_g(T_e) = \int_{\nu_{g-1}}^{\nu_g} b_\nu(\nu, T_e)d\nu, \qquad \sum_{g=1}^{G} b_g = 1,$$

Here we also define the grey Planck opacity

$$\sigma_P = \sum_{g=1}^{G} b_g \sigma_g = \int_0^\infty \sigma_\nu b_\nu d\nu.$$

The group emission opacity σ_g^{em} is a function of ν_{g-1}, ν_g, T_e and σ_ν and can be computed precisely and tabulated without approximations [19]. We refer to appendix D for the practical computation of the opacities terms. On the other hand, σ_g^{abs} is a function of ν_{g-1}, ν_g, T_e but also I_ν. This last dependence is problematic so that different approximations have to be used in practice. At (Planck) equilibrium one has $I_\nu \approx B_\nu(T_e)$, in that case this choice simply leads to $\sigma_g^{abs} = \sigma_g^{em} = \sigma_g$. Another choice consists in taking $I_\nu \approx B_\nu(T_r)$ [19] so that

$$\sigma_g^{abs}(T_e, T_r) = \frac{1}{b_g(T_r)}\int_{\nu_{g-1}}^{\nu_g} \sigma_\nu(\nu, T_e) b_\nu(\nu, T_r)d\nu,$$

which can also be computed accurately and tabulated. Now, by integrating (2) over the unit sphere, one obtains

$$\partial_t \phi_{r,g} + \nabla \cdot F_{r,g} = c\sigma_g(b_g\phi_e - \alpha_g\phi_{r,g}),$$

where

$$\phi_{r,g} = \frac{1}{c}\oint I_g d\omega, \qquad F_{r,g} = \oint I_g \omega d\omega,$$

and α_g is a positive number defined as $\alpha_g = \sigma_g^{abs}/\sigma_g$. The model is said to be at equilibrium if $\forall g \in [1, G],\ \alpha_g = 1$. In the following, in the test problems we work taking $\alpha_g = 1$ but the methodology presented naturally extends to the general case $\alpha_g \neq 1$.

1.3 Model studied and reformulation

The model studied in the present work deals with the time evolution of the ionic, electronic and multigroup radiative energy densities respectively denoted E_i, E_e and $\phi_{r,g}$ in a hot plasma. It writes

$$\begin{cases} \partial_t \phi_{r,g} + \nabla \cdot F_{r,g} = c\sigma_g(b_g\phi_e - \alpha_g\phi_{r,g}) + Q_{r,g}, \quad \forall g \in [1, G], \\ \partial_t E_e = \displaystyle\sum_{g=1}^{G} c\sigma_g(\alpha_g\phi_{r,g} - b_g\phi_e) + c\kappa(T_i - T_e) + Q_e, \\ \partial_t E_i = c\kappa(T_e - T_i) + Q_i. \end{cases} \tag{3}$$

The electron-ion coupling coefficient κ depends on the electronic temperature T_e. Strictly speaking, κ only depending on T_e is true in the weak limit of electron-ion interactions; otherwise, it depends on both T_i, T_e [4]. The total (grey) radiative energy is written $\phi_r = E_r = aT_r^4$ and is given by $\phi_r = \sum_g \phi_{r,g}$, similarly we denote $\phi_\alpha = aT_\alpha^4$ for $\alpha = e, i$. It is supposed that the radiative flux $F_{r,g}$ for the group g follows a diffusion type approximation [19]

$$F_{r,g} = -\frac{c}{3\sigma_g^R(T_e)}\nabla\phi_{r,g}, \tag{4}$$

where σ_g^R denotes the Rosseland (or diffusion) opacity for group g. Now, a reformulation of the model (3) is proposed. It will be shown that it allows to write a very robust and conservative numerical scheme. To do so, the first step consists in writing the model in terms of the quantities ϕ_α. The model can then be written under the form

$$\begin{cases} \partial_t \phi_{r,g} + \nabla \cdot F_{r,g} = c\sigma_g(b_g\phi_e - \alpha_g\phi_{r,g}) + Q_{r,g}, \quad \forall g \in [1, G] \\ \partial_t \phi_e = c\beta_e \displaystyle\sum_{g=1}^{G} \sigma_g(\alpha_g\phi_{r,g} - b_g\phi_e) + \beta_e c\kappa\delta_{ie}(\phi_i - \phi_e) + \beta_e Q_e, \\ \partial_t \phi_i = \beta_i c\kappa\delta_{ie}(\phi_e - \phi_i) + \beta_i Q_i, \end{cases} \tag{5}$$

with

$$\beta_\alpha = \frac{d\phi_\alpha}{dE_\alpha} = \frac{4aT_\alpha^3}{\rho C_{v,\alpha}} > 0, \qquad \rho C_{v,\alpha} = \frac{dE_\alpha}{dT_\alpha}, \qquad \delta_{ie} = \frac{T_i - T_e}{\phi_i - \phi_e} > 0, \qquad \alpha = e, i.$$

The density is denoted ρ and $C_{v,\alpha}$ the heat capacity at constant volume for the population α.

1.4 Properties

The main properties of the model studied are the following

- Total energy conservation.

Adding the three equations of (3) leads to the following total energy balance law

$$\partial_t \left(E_r + E_e + E_i\right) + \nabla.\left(F_r\right) = Q_r + Q_e + Q_i,$$

where we have used the following notations and properties

$$\sum_{g=1}^{G} \phi_{r,g} = \phi_r = aT_r^4, \qquad \sum_{g=1}^{G} Q_{r,g} = Q_r, \qquad \sum_{g=1}^{G} F_{r,g} = F_r.$$

- Maximum principle.

In the case with no source term, if the electronic, ionic and radiative temperatures are bounded at the initial time and at the boundaries then they remain bounded at all time. More precisely if

$$\max\left(T_e(t=0,x), T_i(t=0,x), T_r(t=0,x)\right) \leq K,$$

for $K \in R^{+\star}$ then

$$\max\left(T_e(t,x), T_i(t,x), T_r(t,x)\right) \leq K \quad \forall t \in \mathbb{R}^+.$$

Such a property is studied in [29, 16, 18] and references therein.

- Asymptotic behavior in the limit where σ_g and κ tend to infinity.

In the limit where σ_g and κ tend to infinity system (3) admits a Rosseland equilibrium diffusion limit [19] (where the three temperatures have relaxed towards the same equilibrium temperature).

2 Numerical strategies in the 0D setting

The numerical strategy is now presented for the $0D$ multigroup model (so that spatial derivatives are neglected). It is then extended to the general case.

2.1 First discretisations

Neglecting the spatial derivatives a straightforward backward Euler discretisation of the reformulated model (5) leads to

$$\left\{\begin{array}{l} \phi_{r,g}^{n+1} = \phi_{r,g}^{n} + \Delta t c \sigma_g^{n+1}(b_g^{n+1}\phi_e^{n+1} - \alpha_g^{n+1}\phi_{r,g}^{n+1}) + \Delta t Q_{r,g}, \quad \forall g \in [1,G], \\ \phi_e^{n+1} = \phi_e^{n} + \displaystyle\sum_{g=1}^{G} c\Delta t \beta_e^{n+1}\sigma_g^{n+1}(\alpha_g^{n+1}\phi_{r,g}^{n+1} - b_g^{n+1}\phi_e^{n+1}) + c\Delta t\beta_e^{n+1}\kappa^{n+1}\delta_{ie}^{n+1}(\phi_i^{n+1} - \phi_e^{n+1}) \\ \qquad + \Delta t \beta_e^{n+1} Q_e, \\ \phi_i^{n+1} = \phi_i^{n} + \Delta t \beta_i^{n+1} c\kappa^{n+1}\delta_{ie}^{n+1}(\phi_e^{n+1} - \phi_i^{n+1}) + \Delta t \beta_i^{n+1} Q_i. \end{array}\right. \tag{6}$$

Consequently, the unknown may be written under the convex combination forms

$$\phi_i^{n+1} = \frac{\phi_i^n + \beta_i^{n+1} Q_i \Delta t + \beta_i^{n+1} c\kappa^{n+1} \delta_{ie}^{n+1} \Delta t \phi_e^{n+1}}{1 + \beta_i^{n+1} c\kappa^{n+1} \delta_{ie}^{n+1} \Delta t}, \qquad \phi_{r,g}^{n+1} = \frac{\phi_{r,g}^n + Q_{r,g} \Delta t + c\sigma_g^{n+1} \Delta t b_g^{n+1} \phi_e^{n+1}}{1 + c\sigma_g^{n+1} \alpha_g^{n+1} \Delta t},$$

$$\phi_e^{n+1} = \frac{\psi_e^{n+1} + A^{n+1} \psi_i^{n+1} + \sum_{g=1}^G B_g^{n+1} \psi_{r,g}^{n+1}}{1 + A^{n+1} + \sum_{g=1}^G B_g^{n+1} b_g^{n+1}},$$

where

$$A^{n+1} = \frac{\beta_e^{n+1} c\kappa^{n+1} \delta_{ie}^{n+1} \Delta t}{1 + \beta_i^{n+1} c\kappa^{n+1} \delta_{ie}^{n+1} \Delta t}, \qquad B_g^{n+1} = \beta_e^{n+1} \frac{c\sigma_g^{n+1} \Delta t}{1 + c\sigma_g^{n+1} \alpha_g^{n+1} \Delta t},$$

and

$$\psi_e^{n+1} = \phi_e^n + \beta_e^{n+1} Q_e \Delta t, \qquad \psi_i^{n+1} = \phi_i^n + \beta_i^{n+1} Q_i \Delta t, \qquad \psi_{r,g}^{n+1} = \alpha_g^{n+1} (\phi_{r,g}^n + Q_{r,g} \Delta t),$$

and the following definitions of δ_{ie}^{n+1} and β_α^{n+1}

$$\delta_{ie}^{n+1} = \frac{T_i^{n+1} - T_e^{n+1}}{\phi_i^{n+1} - \phi_e^{n+1}}, \qquad \beta_\alpha^{n+1} = \frac{\phi_\alpha^{n+1} - \phi_\alpha^n}{E_\alpha^{n+1} - E_\alpha^n}, \qquad \alpha = e, i. \tag{7}$$

Remark. We point out that these discrete coefficients are never singular. Indeed, using a straightforward Taylor expansion leads to

$$\lim_{|T_i^{n+1} - T_e^{n+1}| \to 0} \delta_{ie}^{n+1} = \frac{1}{4a(T^{n+1})^3} > 0. \tag{8}$$

Similarly for the coefficients β_α^{n+1}

$$\lim_{|T_\alpha^{n+1} - T_\alpha^n| \to 0} \beta_\alpha^{n+1} = \frac{4aT_\alpha^3}{\rho C_{v,\alpha}(T_\alpha)} > 0. \tag{9}$$

In the following, it will be shown that the discretisation of coefficient β_α^{n+1} is fundamental to enforce a correct discrete energy conservation.

2.2 Practical resolution

Despite the reformulation of the model, the expressions of ϕ_i^{n+1}, ϕ_e^{n+1} and $\phi_{r,g}^{n+1}$ are not completely explicit since they still depend of many implicit parameters. Consequently, in order to proceed with the practical computation iterative methods are presented. To update the solutions from time t^n to t^{n+1} sub-iterations, denoted with the index k, are computed. More precisely, the nonlinear coefficients $\beta_i^{n+1,k}$, $\beta_e^{n+1,k}$, and $\delta_{ie}^{n+1,k}$ are first computed by using (7) then

$$\sigma_g^{n+1,k} = \sigma_g(T_e^{n+1,k}), \qquad \kappa^{n+1,k} = \kappa(T_e^{n+1,k}),$$

as well as

$$\psi_{r,g}^{n+1,k} = \phi_{r,g}^n + Q_{r,g} \Delta t, \quad \psi_e^{n+1,k} = \phi_e^n + \beta_e^{n+1,k} Q_e \Delta t, \quad \psi_i^{n+1,k} = \phi_i^n + \beta_i^{n+1,k} Q_i \Delta t,$$

$$A^{n+1,k} = \frac{\beta_e^{n+1,k} c\kappa^{n+1,k} \delta_{ie}^{n+1,k} \Delta t}{1 + \beta_i^{n+1,k} c\kappa^{n+1,k} \delta_{ie}^{n+1,k} \Delta t}, \qquad B_g^{n+1,k} = \beta_e^{n+1,k} \frac{c\sigma_g^{n+1,k} \Delta t}{1 + c\alpha_g^{n+1,k} \sigma_g^{n+1,k} \Delta t},$$

by using the quantities $(\phi_{r,g}^{n+1,k})$, $\phi_e^{n+1,k}$, $\phi_i^{n+1,k}$. The unknowns $\phi_\alpha^{n+1,k+1}$ are finally updated with

$$\phi_e^{n+1,k+1} = \frac{\psi_e^{n+1,k} + A^{n+1,k}\psi_i^{n+1,k} + \sum_{g=1}^{G} B_g^{n+1,k}\psi_{r,g}^{n+1,k}}{1 + A^{n+1,k} + \sum_{g=1}^{G} B_g^{n+1,k} b_g^{n+1,k}}, \tag{10}$$

$$\phi_i^{n+1,k+1} = \frac{\Psi_i^n + \beta_i^{n+1,k} c\kappa^{n+1,k} \delta_{ie}^{n+1,k} \Delta t \phi_e^{n+1,k+1}}{1 + \beta_i^{n+1,k} c\kappa^{n+1,k} \delta_{ie}^{n+1,k} \Delta t}, \ \phi_{r,g}^{n+1,k+1} = \frac{\psi_{r,g}^{n+1,k} + c\sigma_g^{n+1,k} \Delta t b_g^{n+1,k} \phi_e^{n+1,k+1}}{1 + c\sigma_g^{n+1,k} \alpha_g^k \Delta t}.$$

Regarding the first step ($k = 0$) in the iterative procedure, δ_{ie} is initialized setting $T_i^{n+1,0} = T_i^n$ and $T_e^{n+1,0} = T_e^n$ and (8) if needed. For the coefficients β_α, one considers the limit expression $\beta_\alpha = \dfrac{4a(T_\alpha^n)^3}{\rho C_{v,\alpha}(T_\alpha^n)}$, see (9). The iterative process is repeated until convergence of the scheme. The properties of the scheme are studied in the next section.

2.3 Numerical properties

In this section, the properties of the iterative scheme (10) are studied. More precisely, we focus on the discrete energy conservation, stability and convergence of the scheme.

Property 1 *At convergence of the scheme ($k \to \infty$ so that $\phi^{n+1,k+1} = \phi^{n+1,k} = \phi^{n+1}$), in the case with no source terms ($Q_e = Q_i = Q_{r,g} = 0$), the discrete total energy is conserved.*

Proof.

From the convex combination forms given in equations (2.2), it is not straightforward to obtain the energy conservation relation. However, instead of using the set of equations (2.2), one may start from the set of equations (6) which is equivalent (considering the iterative procedure in k). Summing the $\phi_{r,g}^{n+1,k+1}$ over the groups and adding the resulting equations with the ones on $\phi_i^{n+1,k+1}$ and $\phi_e^{n+1,k+1}$ leads to the following equations

$$\phi_r^{n+1,k+1} - \phi_r^n + \frac{\phi_e^{n+1,k+1} - \phi_e^n}{\beta_e^{n+1,k}} + \frac{\phi_i^{n+1,k+1} - \phi_i^n}{\beta_i^{n+1,k}} = 0.$$

Then, by using the definition of $\beta_\alpha^{n+1,k}$ given in (7) leads to the discrete energy conservation (when k tends to infinity)

$$E_r^{n+1} + E_e^{n+1} + E_i^{n+1} = E_r^n + E_e^n + E_i^n.$$

Remark. As pointed out, the discretisation of the coefficients β_α given in (7) are crucial here to obtain the correct conservation property.

Property 2 *The scheme* (10) *is unconditionally* L^∞ *stable at each sub-iterate* k.

Proof.
Remarking that the coefficients $A^{n+1,k}$, $B^{n+1,k}$ and $b_g^{n+1,k}$ are positive then, according to (10), $\phi_e^{n+1,k+1}$ writes under the form of a convex combination of $\psi_e^{n+1,k}$, $\psi_i^{n+1,k}$, $(\psi_{r,g}^{n+1,k}/b_g^{n+1,k})_{g\in[1,G]}$. Therefore, defining $\psi_{min}^{n+1,k}$ and $\psi_{max}^{n+1,k}$ as

$$\psi_{min}^{n+1,k} = \min\left(\psi_e^{n+1,k}, \psi_i^{n+1,k}, \left(\frac{\psi_{r,g}^{n+1,k}}{b_g^{n+1,k}}\right)\right), \quad \psi_{max}^{n+1,k} = \max\left(\psi_e^{n+1,k}, \psi_i^{n+1,k}, \left(\frac{\psi_{r,g}^{n+1,k}}{b_g^{n+1,k}}\right)\right),$$

we have the following estimates

$$\psi_{min}^{n+1,k} \leq \phi_e^{n+1,k+1} \leq \psi_{max}^{n+1,k}.$$

In addition, since the parameters $\beta_i^{n+1,k}$, $\kappa^{n+1,k}$ and $\delta_{ie}^{n+1,k}$ are also positive, equation (6) shows that $\phi_i^{n+1,k+1}$ also writes as a convex combination of $\psi_i^{n+1,k}$ and $\phi_e^{n+1,k+1}$. Consequently, it follows that

$$\psi_{min}^{n+1,k} \leq \phi_i^{n+1,k+1} \leq \psi_{max}^{n+1,k}.$$

Moreover, equation (6) also gives the convex combination

$$\phi_{r,g}^{n+1,k+1} = \frac{\phi_{r,g}^n + Q_{r,g}\Delta t + c\sigma_g^{n+1,k}\Delta t b_g^{n+1,k}\phi_e^{n+1,k+1}}{1 + c\sigma_g^{n+1,k}\alpha_g^{n+1,k}\Delta t} = \frac{b_g^{n+1,k}}{\alpha_g^{n+1,k}} \frac{\frac{\psi_{r,g}^{n+1,k}}{\alpha_g^{n+1,k} b_g^{n+1,k}} + c\sigma_g^{n+1,k}\Delta t\phi_e^{n+1,k+1}}{\frac{1}{\alpha_g^{n+1,k}} + c\sigma_g^{n+1,k}\Delta t}.$$

where $\sigma_g^{n+1,k}$ and $\alpha_g^{n+1,k}$ are positive. Hence,

$$\forall g \in [1,G], \qquad \frac{b_g^{n+1,k}}{\alpha_g^{n+1,k}}\psi_{min}^{n+1,k} \leq \phi_{r,g}^{n+1,k+1} \leq \frac{b_g^{n+1,k}}{\alpha_g^{n+1,k}}\psi_{max}^{n+1,k}.$$

In the classic case ($\alpha_g = 1$), by summing the previous inequality over all the groups and using the fact that $\sum_{g=1}^G b_g^{n+1,k} = 1$ leads to

$$\psi_{min}^{n+1,k} \leq \phi_r^{n+1,k+1} \leq \psi_{max}^{n+1,k}.$$

Property 3 *(Convergence) If* Δt *is small enough, the sequence* $\left\{\phi^{n+1,k}\right\}_k = (\phi_{r,1}^{n+1,k}, \cdots, \phi_{r,G}^{n+1,k}, \phi_e^{n+1,k}, \phi_i^{n+1,k})$ *defined in (10) converges toward* ϕ^{n+1} *solution of (6).*

Proof.
In the $0D$ setting, system (5) can be written as

$$\dot{\phi} = A(\phi)\phi + Q(\phi), \tag{11}$$

with

$$\phi = \begin{pmatrix} \phi_{r,1} \\ \vdots \\ \phi_{r,G} \\ \phi_e \\ \phi_i \end{pmatrix}, \qquad Q(\phi) = \begin{pmatrix} Q_{r,1} \\ \vdots \\ Q_{r,G} \\ \beta_e Q_e \\ \beta_i Q_i \end{pmatrix},$$

and

$$A(\phi) = c \begin{pmatrix} -\sigma_1\alpha_1 & \dots & 0 & \sigma_1 b_1 & 0 \\ \vdots & \ddots & \vdots & \vdots & \vdots \\ 0 & \dots & -\sigma_G\alpha_G & \sigma_G b_G & 0 \\ \beta_e\sigma_1\alpha_1 & \dots & \beta_e\sigma_G\alpha_G & \beta_e\left(-\sum_{g=1}^{G}\sigma_g b_g - \kappa\delta_{ie}\right) & \beta_e\kappa\delta_{ie} \\ 0 & \dots & 0 & \beta_i\kappa\delta_{ie} & -\beta_i\kappa\delta_{ie} \end{pmatrix}.$$

System (6) is a Euler backward time discretisation of the system (11) and is given by

$$\phi^{n+1} = \phi^n + \Delta t Q(\phi^{n+1}) + \Delta t A(\phi^{n+1})\phi^{n+1}, \quad \phi^{n+1} = \left(I - \Delta t A\left(\phi^{n+1}\right)\right)^{-1}\left(\phi^n + \Delta t Q\left(\phi^{n+1}\right)\right).$$

The iterative method writes

$$\phi^{n+1,k+1} = f_n(\phi^{n+1,k}), \quad f_n(\phi) = (I - \Delta t A(\phi))^{-1}(\phi^n + \Delta t Q(\phi)), \quad \phi^{n+1,0} = \phi^n.$$

Since the scheme is stable, the numerical solution $(\phi^n)_{n\in\mathbb{N}}$ remains in a compact convex subset of $\mathbb{R}^{G+2}$ named E. Since A is smooth, it holds $||A||_\infty := \max_{\phi\in E} ||A(\phi)|| < \infty$ and for $\Delta t < ||A||_\infty^{-1}$ one can write

$$\forall \phi \in E,\ (I - \Delta t A(\phi))^{-1} = I + \sum_{i=1}^{\infty} (\Delta t)^i A(\phi)^i,$$

and

$$f_n(\phi) = \phi^n + \Delta t H_n(\phi), \qquad H_n(\phi) = Q(\phi) + \sum_{i=1}^{\infty} (\Delta t)^{i-1} A(\phi)^i (\phi^n + \Delta t Q(\phi)).$$

Using the mean value theorem (since A and H_n are smooth and the time step is bounded $0 \le \Delta t \le (\Delta t)_{max} < ||A||_\infty$), there exists a positive constant K (independent of Δt and n) such that

$$\forall (\phi_1, \phi_2) \in E^2,\ ||H_n(\phi_1) - H_n(\phi_2)|| \le K||\phi_1 - \phi_2||,$$

thus

$$\forall (\phi_1, \phi_2) \in E^2,\ ||f_n(\phi_1) - f_n(\phi_2)|| \le \Delta t K||\phi_1 - \phi_2||.$$

Thus, for Δt small enough, the mapping $f_n : \phi^{n+1,k} \mapsto \phi^{n+1,k+1}$ is a contraction mapping. This property guarantees that the sequence $(\phi^{n+1,k})_{k\in\mathbb{N}}$ converges to the unique fixed point of f_n, which is the solution of system (6).

Remark. Following exactly the procedure already presented in [8] by using discrete Hilbert expansions, it is possible to show that the numerical scheme presented here is asymptotic-preserving in the limit σ_P and κ tend to infinity.

3 $1D$ multigroup model

In this section, we add the contribution of the radiation flux (diffusion approximation) in the simplified case of one spatial dimension. The numerical procedure presented in the 0D case is extended then the resulting scheme is analyzed.

3.1 1D model and associated numerical scheme

In the one dimensional setting, the reformulated scheme writes as follows

$$\begin{cases} \partial_t \phi_{r,g} + \partial_x (F_{r,g}) = c\sigma_g (b_g \phi_e - \phi_{r,g}) + Q_{r,g}, \quad \forall g \in [1, G], \\ \partial_t \phi_e = \displaystyle\sum_{g=1}^{G} c\beta_e \sigma_g (\phi_{r,g} - b_g \phi_e) + c\kappa\beta_e \delta_{ie} (\phi_i - \phi_e) + \beta_e Q_e, \\ \partial_t \phi_i = c\kappa\beta_i \delta_{ie} (\phi_e - \phi_i) + \beta_i Q_i, \end{cases} \tag{12}$$

where for clarity we have set $\alpha_g = 1$ but the methodology presented holds in the general case. The radiation flux considered writes

$$F_{r,g} = -\frac{c}{3\sigma_g^R} \partial_x \phi_{r,g}, \quad \forall g \in [1, G].$$

For the space discretisation we introduce the space interval $[0, L]$ divided in M uniform cells. Denote $j \in [1, M]$ the index of a cell. A standard three points diffusion scheme (1D) is considered

$$(\partial_x F_{r,g})_j = \frac{F_{r,g,j+1/2} - F_{r,g,j-1/2}}{\Delta x}, \qquad F_{r,g,j+1/2} = -\frac{c}{3\sigma_{g,j+1/2}^R \Delta x} (\phi_{r,g,j+1} - \phi_{r,g,j}),$$

with $\Delta x = L/M$. Therefore we have, far from the boundaries,

$$\Delta t (\partial_x F_{r,g})_j^{n+1} = -\Delta t \lambda_{g,j+1/2}^{n+1} (\phi_{r,g,j+1}^{n+1} - \phi_{r,g,j}^{n+1}) + \Delta t \lambda_{g,j-1/2}^{n+1} (\phi_{r,g,j}^{n+1} - \phi_{r,g,j-1}^{n+1}),$$

where

$$\lambda_{g,j+1/2}^{n+1} = \frac{c}{3(\sigma_{g,j+1/2}^R)^{n+1} (\Delta x)^2}, \qquad \sigma_{g,j+1/2}^R = \sigma_g^R \left(\frac{T_{e,j} + T_{e,j+1}}{2} \right).$$

The 0D scheme naturally extends to write

$$\begin{cases} \phi_{r,g,j}^{n+1} + \Delta t (\partial_x F_{r,g})_j^{n+1} = \phi_{r,g,j}^n + \Delta t c \sigma_{g,j}^{n+1} (b_{g,j}^{n+1} \phi_{e,j}^{n+1} - \phi_{r,g,j}^{n+1}), \quad \forall g \in [1, G], \\ \phi_{e,j}^{n+1} = \phi_{e,j}^n + \displaystyle\sum_{g=1}^{G} c\Delta t \beta_{e,j}^{n+1} \sigma_{g,j}^{n+1} (\phi_{r,g,j}^{n+1} - b_{g,j}^{n+1} \phi_{e,j}^{n+1}) + c\Delta t \beta_{e,j}^{n+1} \kappa_j^{n+1} \delta_{ie,j}^{n+1} (\phi_{i,j}^{n+1} - \phi_{e,j}^{n+1}), \\ \phi_{i,j}^{n+1} = \phi_{i,j}^n + \Delta t \beta_{i,j}^{n+1} c \kappa_j^{n+1} \delta_{ie,j}^{n+1} (\phi_{e,j}^{n+1} - \phi_{i,j}^{n+1}). \end{cases} \tag{13}$$

The last equation of (13) can be reformulated to write under the convex combination form

$$\phi_{i,j}^{n+1} = h_j^{n+1} \phi_{i,j}^n + (1 - h_j^{n+1}) \phi_{e,j}^{n+1}, \qquad h_j^{n+1} = \frac{1}{1 + c\beta_{i,j}^{n+1} \delta_{ie,j}^{n+1} \kappa_j^{n+1} \Delta t}.$$

Now, we introduce the notation

$$H_j^{n+1} = c\Delta t \beta_{e,j}^{n+1} \delta_{ie,j}^{n+1} \kappa_j^{n+1} h_j^{n+1}, \tag{14}$$

so that the second equation of system (13) reads

$$\phi_{e,j}^{n+1} = \phi_{e,j}^n + c\Delta t \beta_{e,j}^{n+1} \sum_{g=1}^{G} \sigma_{g,j}^{n+1} \phi_{r,g,j}^{n+1} - c\Delta t \beta_{e,j}^{n+1} \sigma_{P,j}^{n+1} \phi_{e,j}^{n+1} + H_j^{n+1} (\phi_{i,j}^n - \phi_{e,j}^{n+1}), \tag{15}$$

where we have used the fact that

$$\sum_{g=1}^{G} \sigma_{g,j}^{n+1} b_{g,j}^{n+1} = \sigma_{P,j}^{n+1}.$$

Similarly, by defining $R_{g,j}^{n+1} = c\Delta t \beta_{e,j}^{n+1} \sigma_{g,j}^{n+1}$, equation (15) writes under the compact form

$$\phi_{e,j}^{n+1} = \frac{\phi_{e,j}^n + H_j^{n+1} \phi_{i,j}^n + \sum_{g=1}^{G} R_{g,j}^{n+1} \phi_{r,g,j}^{n+1}}{1 + H_j^{n+1} + c\Delta t \beta_{e,j}^{n+1} \sigma_P^{n+1}}. \tag{16}$$

Finally, thanks to (16), the first G equations of (13) write

$$\begin{aligned} \phi_{r,g,j}^{n+1} (1 + c\sigma_{g,j}^{n+1} \Delta t) - c\sigma_{g,j}^{n+1} b_{g,j}^{n+1} \Delta t \frac{\sum_{g'=1}^{G} R_{g',j}^{n+1} \phi_{r,g',j}^{n+1}}{1 + H_j^{n+1} + c\Delta t \beta_{e,j}^{n+1} \sigma_P^{n+1}} + \Delta t (\partial_x F_{r,g})_j^{n+1} \\ = \phi_{r,g,j}^n + c\sigma_{g,j}^{n+1} b_{g,j}^{n+1} \Delta t \frac{\phi_{e,j}^n + H_j^{n+1} \phi_{i,j}^n}{1 + H_j^{n+1} + c\Delta t \beta_{e,j}^{n+1} \sigma_{P,j}^{n+1}}. \end{aligned} \tag{17}$$

Besides, by defining

$$C_j = \frac{c\Delta t \left(\phi_{e,j}^n + H_j^{n+1} \phi_{i,j}^n \right)}{1 + H_j^{n+1} + c\Delta t \beta_{e,j}^{n+1} \sigma_P^{n+1}}, \qquad K_j = \frac{(c\Delta t)^2 \beta_{e,j}^{n+1}}{1 + H_j^{n+1} + c\Delta t \beta_{e,j}^{n+1} \sigma_P^{n+1}},$$

it is then possible to write (17) as follows

$$\begin{aligned} \phi_{r,g,j}^{n+1} (1 + c\sigma_{g,j}^{n+1} \Delta t) - K_j \sigma_{g,j}^{n+1} b_{g,j}^{n+1} \sum_{g'=1}^{G} \sigma_{g',j}^{n+1} \phi_{r,g',j}^{n+1} + \Delta t (\partial_x F_{r,g})_j^{n+1} \\ = \phi_{r,g,j}^n + C_j \sigma_{g,j}^{n+1} b_{g,j}^{n+1}, \end{aligned}$$

so that (17) rewrites under the non linear system form

$$A_{total}^{n+1} \begin{pmatrix} \Phi_{r,1}^{n+1} \\ \vdots \\ \Phi_{r,M}^{n+1} \end{pmatrix} = \begin{pmatrix} Y_1^{n+1} + \Phi_{r,1}^n \\ \vdots \\ Y_M^{n+1} + \Phi_{r,M}^n \end{pmatrix}, \tag{18}$$

where

$$A_{total}^{n+1} = \begin{pmatrix} A_1^{n+1} + c_1^{n+1} & -c_1^{n+1} & 0 & \cdot \\ -c_1^{n+1} & A_2^{n+1} + c_1^{n+1} + c_2^{n+1} & -c_2^{n+1} & \cdots \\ 0 & \ddots & \ddots & -c_{M-1}^{n+1} \\ 0 & 0 & -c_{M-1}^{n+1} & A_M^{n+1} + c_{M-1}^{n+1} \end{pmatrix}, \tag{19}$$

and we have defined the matrices

$$A_j^{n+1} = \begin{pmatrix} 1 + c\Delta t \sigma_{1,j}^{n+1} & 0 & 0 \\ 0 & \ddots & 0 \\ 0 & 0 & 1 + c\Delta t \sigma_{G,j}^{n+1} \end{pmatrix} - K_j \begin{pmatrix} b_{1,j}^{n+1}\sigma_{1,j}^{n+1}\sigma_{1,j}^{n+1} & \cdots & b_{1,j}^{n+1}\sigma_{1,j}^{n+1}\sigma_{G,j}^{n+1} \\ \vdots & \vdots & \vdots \\ b_{G,j}^{n+1}\sigma_{G,j}^{n+1}\sigma_{1,j}^{n+1} & \cdots & b_{G,j}^{n+1}\sigma_{G,j}^{n+1}\sigma_{G,j}^{n+1} \end{pmatrix},$$

as well as the vectors $\Phi_{r,j}^{n+1}$ and Y_j^{n+1}

$$\Phi_{r,j}^{n+1} = \begin{pmatrix} \phi_{r,1,j}^{n+1} \\ \vdots \\ \phi_{r,G,j}^{n+1} \end{pmatrix}, \quad Y_j^{n+1} = C_j \begin{pmatrix} b_{1,j}^{n+1}\sigma_{1,j}^{n+1} \\ \vdots \\ b_{G,j}^{n+1}\sigma_{G,j}^{n+1} \end{pmatrix},$$

and the diffusion matrix

$$c_j^{n+1} = \Delta t \begin{pmatrix} \lambda_{1,j+1/2}^{n+1} & 0 & 0 \\ 0 & \ddots & 0 \\ 0 & 0 & \lambda_{G,j+1/2}^{n+1} \end{pmatrix}.$$

We point out that the matrices A_j may be expanded as follows

$$A_j^{n+1} = D_j^{n+1} + M_j^{n+1}, \quad D_j^{n+1} = \mathrm{diag}(1 + c\Delta t \sigma_{1,j}^{n+1}, \cdots, 1 + c\Delta t \sigma_{G,j}^{n+1}),$$

and the matrices M_j

$$(M_j^{n+1})_{g,g'} = -K_j b_{g,j}^{n+1} \sigma_{g,j}^{n+1} \sigma_{g',j}^{n+1},$$

may be written as the tensor product of two vectors u_j and v_j

$$M_j^{n+1} = u_j^{n+1} \otimes v_j^{n+1}, \quad u_j^{n+1} = -K_j \begin{pmatrix} \sigma_{1,j}^{n+1} b_{1,j}^{n+1} \\ \vdots \\ \sigma_{G,j}^{n+1} b_{G,j}^{n+1} \end{pmatrix}, \quad v_j^{n+1} = \begin{pmatrix} \sigma_{1,j}^{n+1} \\ \vdots \\ \sigma_{G,j}^{n+1} \end{pmatrix}.$$

In the next section, it will be shown that this property is useful to prove that the matrices A_j^{n+1} are invertible and their inverse may be easily computed.

3.2 Numerical properties and practical resolution

The numerical properties of the 1D scheme are now given. We first recall the following result which is particularly useful for the practical resolution of the 1D scheme.

Property 1 *(Sherman-Morrison formula)* Let $\tilde{A} \in \mathbb{R}^{G\times G}$ be an invertible matrix and $u,\ v \in \mathbb{R}^G$ such as $1 + v^T\tilde{A}^{-1}u \neq 0$. Therefore $\tilde{A} + u \otimes v$ is invertible and its inverse is

$$(\tilde{A} + u \otimes v)^{-1} = \tilde{A}^{-1} - \frac{\tilde{A}^{-1}u \otimes v\tilde{A}^{-1}}{1 + v^T\tilde{A}^{-1}u}. \tag{20}$$

This property enables to easily compute the inverse of the matrices $(A_j)_{j\in[1,M]}$.

Definition Let $P \in \mathbb{R}^{N\times N}$. P is a M-matrix if

$$\begin{cases} P_{i,j} \leq 0, \quad i \neq j \quad \forall (i,j) \in [1,N]^2, \\ \displaystyle\sum_{j=1}^{N} P_{i,j} \geq 0, \quad \forall i \in [1,N]. \end{cases}$$

In addition, P is a strict M-matrix if $\displaystyle\sum_{j=1}^{N} P_{i,j} > 0, \qquad \forall i \in [1,N]$.

Property 2 *Let $P \in \mathbb{R}^{N\times N}$ be a strict M-matrix. Hence P is invertible and its inverse has non negative coefficients.*

Property 3 *The coefficients of the inverse of the matrix of system (18), namely $(A_{total}^{n+1})^{-1}$, are non negative.*

Proof. It is equivalent to prove that $(A_{total}^{n+1})^T$ is a strict M-matrix. The sum over the column g of A_{total}^{n+1} gives $1 + c\Delta t\sigma_g^{n+1} - K_j\sigma_P^{n+1}\sigma_g^{n+1}$. Since $H_j^{n+1} > 0$ hence $K_j\sigma_P^{n+1} < c\Delta t$. Therefore, because of Property 2, the coefficients of $((A_{total}^{n+1})^T)^{-1} = ((A_{total}^{n+1})^{-1})^T$ are non negative. As a consequence, $(A_{total}^{n+1})^{-1}$ has non negative coefficients.

Since the components of the right hand-side of (18) are positive this property enables to show the positivity of the discrete solution $(\phi_{r,g}^n)_{n\in\mathbb{N}}$.

3.3 1D discretisation with source terms

The previous expressed can be extended to include the contribution of external source terms. In this case, the following expressions are obtained

$$\phi_{i,j}^{n+1} = h_j^{n+1}\psi_{i,j}^n + (1 - h_j^{n+1})\phi_{e,j}^{n+1}, \qquad \phi_{e,j}^{n+1} = \frac{\psi_{e,j}^n + H_j^{n+1}\psi_{i,j}^n + \sum_{g=1}^{G} R_{g,j}^{n+1}\phi_{r,g,j}^{n+1}}{1 + H_j^{n+1} + c\Delta t\beta_{e,j}^{n+1}\sigma_{P,j}^{n+1}}, \tag{21}$$

$$C_j = \frac{c\Delta t\left(\psi_{e,j}^n + H_j^{n+1}\psi_{i,j}^n\right)}{1 + H_j^{n+1} + c\Delta t\beta_{e,j}^{n+1}\sigma_{P,j}^{n+1}}, \qquad A_{total}^{n+1}\begin{pmatrix}\Phi_{r,1}^{n+1}\\ \vdots \\ \Phi_{r,M}^{n+1}\end{pmatrix} = \begin{pmatrix} Y_1^{n+1} + \Psi_{r,1}^n \\ \vdots \\ Y_M^{n+1} + \Psi_{r,M}^n\end{pmatrix}, \tag{22}$$

where H_j^{n+1} and A_{total}^{n+1} are respectively defined in (14) and (19).

System (22) may be solved using standard iterative techniques such that Jacobi, Gauss-Seidel or bi-conjugate gradient strategies. In that case, property (20) may be used extensively to easily compute the inverse of the matrices A_j (at least for Jacobi or Gauss-Seidel). In practice, to update the numerical solution from time t^n to t^{n+1}, sub-iterations in k are considered. We start by computing the $\Phi_r^{n+1,k+1}$ terms by solving the set of equations (22). Then $\phi_{e,j}^{n+1,k+1}$ and $\phi_{i,j}^{n+1,k+1}$ are updated with equations (21). In this process the nonlinear coupling terms Y_j, h_j, H_j, $R_{g,j}$, $\beta_{e,j}$ and the coefficients in the matrix A_{total} are fixed at sub-iteration k to enable convex-combination forms leading to strong stability properties. However, despite the interesting properties which may be proven here, the size of the matrices involved may be problematic. Indeed a direct resolution becomes particularly expensive when working with a large number of cells and frequency groups. In the next section a decoupling strategy is presented to address this issue.

3.4 Decoupling procedure

A direct inversion of system (18) requires to solve non-symmetric linear systems of size $(G\times M)^2$ many times at each time iteration. This may be not affordable when considering realistic applications. In order to overcome this difficulty, a decoupling of the diffusion terms and the groups coupling terms is used. In practice, the method comes down to solving G $(M \times M)$ tridiagonal symmetric systems. More precisely, the idea is to chose the group-coupling terms at sub-iteration k while keeping the $\phi_{r,g,j}$ in the diffusion terms at sub-iteration $k+1$ as follows

$$\phi_{r,g,j}^{n+1,k+1} + \Delta t(\partial_x F_{r,g})_j^{n+1,k+1} = \phi_{r,g,j}^n + c\Delta t\sigma_{g,j}^{n+1,k}(b_{g,j}^{n+1,k}\phi_{e,j}^{n+1,k} - \phi_{r,g,j}^{n+1,k+1}).$$

The coefficients λ in the diffusion term are intentionally fixed at iteration k to avoid a nonlinear dependence on ϕ_e. The associated numerical scheme then writes

$$\begin{aligned}\phi_{r,g,j}^{n+1,k+1}(1 + c\sigma_{g,j}^{n+1,k}\Delta t + \Delta t\lambda_{g,j-1/2}^{n+1,k} + \Delta t\lambda_{g,j+1/2}^{n+1,k}) - \Delta t\lambda_{g,j-1/2}^{n+1,k}\phi_{r,g,j-1}^{n+1,k+1} - \Delta t\lambda_{g,j+1/2}^{n+1,k}\phi_{r,g,j+1}^{n+1,k+1}\\ = \phi_{r,g,j}^n + c\sigma_{g,j}^{n+1,k}b_{g,j}^{n+1,k}\Delta t\phi_{e,j}^{n+1,k},\end{aligned}$$

which rewrites

$$\begin{pmatrix} a_{g,1}^{n+1,k} & c_{g,1}^{n+1,k} & 0 & \cdots & 0 \\ c_{g,1}^{n+1,k} & a_{g,2}^{n+1,k} & c_{g,2}^{n+1,k} & & \vdots \\ 0 & \ddots & \ddots & \ddots & 0 \\ \vdots & & c_{g,M-2}^{n+1,k} & a_{g,M-1}^{n+1,k} & c_{g,M-1}^{n+1,k} \\ 0 & \cdots & 0 & c_{g,M-1}^{n+1,k} & a_{g,M}^{n+1,k} \end{pmatrix} \begin{pmatrix} \phi_{r,g,1}^{n+1,k+1} \\ \\ \vdots \\ \\ \phi_{r,g,M}^{n+1,k+1} \end{pmatrix} = \begin{pmatrix} y_{g,1}^{n+1,k} \\ \\ \vdots \\ \\ y_{g,M}^{n+1,k} \end{pmatrix}, \quad \forall g \in [1, G], \tag{23}$$

with

$$a_{g,j}^{n+1,k} = 1 + c\sigma_{g,j}^{n+1,k}\Delta t + \Delta t\lambda_{g,j-1/2}^{n+1,k} + \Delta t\lambda_{g,j+1/2}^{n+1,k}, \qquad c_{g,j}^{n+1,k} = -\Delta t\lambda_{g,j+1/2}^{n+1,k},$$

and

$$y_{g,j}^{n+1,k} = \phi_{r,g}^{n} + c\sigma_{g}^{n+1,k} b_{g}^{n+1,k}\Delta t\phi_{e}^{n+1,k}.$$

In practice, these G linear systems are solved using a conjugate gradient algorithm to obtained the $\phi_{r,g,j}^{n+1,k+1}$ terms. The $\phi_{e,j}^{n+1,k+1}$ and $\phi_{i,j}^{n+1,k+1}$ terms are then updated with the following equations

$$\phi_{e,j}^{n+1,k+1} = \frac{\psi_{e,j}^{n} + H_{j}^{n+1,k}\psi_{i,j}^{n} + \sum_{g=1}^{G} R_{g,j}^{n+1,k}\phi_{r,g,j}^{n+1,k+1}}{1 + H_{j}^{n+1,k} + c\Delta t\beta_{e,j}^{n+1,k}\sigma_{P,j}^{n+1,k}}, \tag{24}$$

and

$$\phi_{i,j}^{n+1,k+1} = h_{j}^{n+1,k}\psi_{i,j}^{n} + (1 - h_{j}^{n+1,k})\phi_{e,j}^{n+1,k+1}. \tag{25}$$

In order to enhance the convergence speed of this iterative procedure, the initial condition (initial guess) may be adapted. This point is discussed in detail in Appendix. In addition, in the spirit of [22, 9], acceleration methods may be used. This point is also discussed in Appendix.

Remark. In the present study, electron and ion conduction terms have been neglected. These terms add spatial coupling to the Φ_e and Φ_i evolution equations. When it is possible, a simple approach to take electron and ion conductivities into account is to use a simple splitting operator strategy. If it is not possible (i.e. if the numerical error due to the splitting procedure becomes too large) the decoupling strategy presented here still enables to compute the $\phi_{r,g}^{n+1,k+1}$ terms (by solving G $M \times M$ set of equations) then compute the $\phi_{i}^{n+1,k+1}$ and $\phi_{e}^{n+1,k+1}$ terms (by solving a $2M \times 2M$ system) at each sub-iterations. Of course, by lagging the $\phi_{i}^{n+1,k+1}$ terms at sub-iteration k in the $\phi_{e}^{n+1,k+1}$ evolution equation enables to solve two $M \times M$ systems to update $\phi_{e}^{n+1,k+1}$ then $\phi_{i}^{n+1,k+1}$.

3.5 Properties

In this section, the properties of the decoupling procedure are given. In particular we highlight that despite the decoupling procedure adopted here the positivity of the discrete solution is ensured.

Property 1 *The matrix of system* (23) *is a strict M-matrix.*
Since the components of the left hand-side of (23) are positive. This property guarantees that the numerical solution remains positive.

Property 2 *(Gershgorin's lemma)* Let $A \in \mathbb{C}^{M\times M}$ and λ an eigenvalue of A. There exists $j \in [1, M]$ such that

$$|\lambda - a_{j,j}| \leq \sum_{i\neq j} |a_{i,j}|. \tag{26}$$

Property 3 *(Stability) The following estimate holds for each sub-iteration and for all* $g \in [1, G]$

$$\max_{j\in[1,M]} \phi^{k+1}_{r,g,j} \leq \sqrt{M} \max_{j\in[1,M]} \gamma^{n+1,k}_{g,j}, \qquad \gamma^{n+1,k}_{g,j} = \frac{\phi^n_{r,g,j} + c\sigma^{n+1,k}_{g,j} b^{n+1,k}_{g,j} \Delta t \phi^{n+1,k}_{e,j}}{1 + c\sigma^{n+1,k}_{g,j}\Delta t}.$$

Proof. Dividing the j-*th* line by $1 + c\sigma^{n+1,k}_{g,j}\Delta t$, system (23) rewrites

$$\begin{aligned}
&\begin{pmatrix} 1+c'_0+c'_1 & -c'_1 & & 0 \\ -c'_1 & 1+c'_1+c'_2 & -c'_2 & \\ & \ddots & \ddots & \ddots \\ 0 & & -c'_{M-1} & 1+c'_{M-1}+c'_M \end{pmatrix} \begin{pmatrix} \phi^{n+1,k+1}_{r,g,1} \\ \vdots \\ \phi^{n+1,k+1}_{r,g,M} \end{pmatrix} \\
&\equiv A^k_g \begin{pmatrix} \phi^{n+1,k+1}_{r,g,1} \\ \vdots \\ \phi^{n+1,k+1}_{r,g,M} \end{pmatrix} = \begin{pmatrix} \gamma^{n+1,k}_{g,1} \\ \vdots \\ \gamma^{n+1,k}_{g,M} \end{pmatrix}
\end{aligned} \tag{27}$$

with

$$c'_j = \frac{\Delta t \lambda^{n+1,k}_{g,j+1/2}}{1 + c\sigma^{n+1,k}_{g,j}\Delta t}, \qquad \gamma^{n+1,k}_{g,j} = \frac{\phi^n_{r,g,j} + c\sigma^{n+1,k}_{g,j} b^{n+1,k}_{g,j} \Delta t \phi^{n+1,k}_{e,j}}{1 + c\sigma^{n+1,k}_{g,j}\Delta t}.$$

The matrix A^k_g is real symmetric, hence it can be diagonalised and its eigenvalues are real. Let λ be an eigenvalue then according to the inequality (26), there exists $j \in [1, M]$ such that

$$|1 + c'_j + c'_{j+1} - \lambda| = |c'_j + c'_{j+1} - (\lambda - 1)| \leq c'_j + c'_{j+1},$$

and thus $\lambda - 1 \geq 0$. Besides λ^{-1} is an eigenvalue of $(A_g^k)^{-1}$ and $\lambda^{-1} \leq 1$. Therefore as $(A_g^k)^{-1}$ can also be diagonalised

$$||(A_g^k)^{-1}||_2 = \max_{\lambda' \in Sp((A_g^k)^{-1})} |\lambda'| \leq 1.$$

Finally by denoting

$$\Phi_g^{k+1} = \begin{pmatrix} \phi_{r,g,1}^{n+1,k+1} \\ \vdots \\ \phi_{r,g,M}^{n+1,k+1} \end{pmatrix}, \qquad \Gamma_g^k = \begin{pmatrix} \gamma_{g,1}^{n+1,k} \\ \vdots \\ \gamma_{g,M}^{n+1,k} \end{pmatrix},$$

one can write

$$A_g^k \Phi_g^{k+1} = \Gamma_g^k, \qquad \Phi_g^{k+1} = (A_g^k)^{-1} \Gamma_g^k,$$

and therefore

$$||\Phi_g^{k+1}||_2 = ||(A_g^k)^{-1}\Gamma_g^k||_2 \leq ||(A_g^k)^{-1}||_2 \; ||\Gamma_g^k||_2 \leq ||\Gamma_g^k||_2.$$

Furthermore, for any vector $X \in \mathbb{R}^M$, it holds

$$||X||_\infty \leq ||X||_2 \leq \sqrt{M}||X||_\infty.$$

Finally the following inequalities are obtained

$$||\Phi_g^{k+1}||_\infty \leq ||\Phi_g^{k+1}||_2 \leq ||\Gamma_g^k||_2 \leq \sqrt{M}||\Gamma_g^k||_\infty.$$

Property 5 *(Convergence) If Δt is small enough, then the sequence $\phi^{n+1,k} = (\phi_{r,g,j}^{n+1,k}, \phi_{e,j}^{n+1,k}, \phi_{i,j}^{n+1,k})$ converges toward ϕ^{n+1} which is solution of (18).*

Proof. The proof of convergence for this procedure exactly relies on the same arguments that were developed for the $0D$ case.

Remark. The decoupling procedure is not particularly new and the resolution of a $(GM)^2$ system may be handle in an HPC context. Here we focus on the robustness of the decoupled algorithm and its interesting numerical properties. If the computing resources available allow a direct resolution of the full system (without decoupling procedure), then the decoupling procedure is not mandatory. However, because of the coupling with matter (here ions and electrons), the system of equations becomes strongly non-linear and a non-symmetric $(GM)^2$ system needs to be solved at each sub-iteration (so many times at each time iteration). We believe this may become problematic with a very large number of groups and cells even with powerful computing resources. In addition, the procedure presented here naturally apply to unstructured meshes. In this case, depending on the space discretisation of the implicit diffusion terms chosen, the complexity of the non-symmetric matrix structure may be largely increased. This raises

the numerical cost involved when solving the large $(GM)^2$ system and significantly increases the cost of the full iterative process at each time iteration. Also, the decoupling procedure also enables the use of acceleration techniques in the spirit of [23, 9] as presented in Appendix. For these reasons, we believe the decoupling procedure with its numerical properties is of interest to the community.

4 Numerical results

In this section, numerical experiments are now presented to demonstrate the correct behavior of the studied methods. All the numerical tests are carried out with the numerical scheme (23) (scheme obtained with the decoupling procedure). Indeed, as pointed out in the previous section, a direct resolution of (18) is not affordable when working with a large number of cells or frequency groups. We mention here that the groups distribution is distributed logarithmically. More precisely, in practice we work with

$$\ln(\nu_{g+1}) = \ln(\nu_g) + K,$$

with $K = \log(\nu_G/\nu_0)/G$ and $\nu_0 = 4.88 \cdot 10^{-8}$ and $\nu_G = 1.0874 \cdot 10^8$.

4.1 $0D$ slab

We start this section by focusing on 0D (no spatial variation) numerical experiments. This series of tests cases is taken from [8, 10] and adapted to the present multigroup context. Here the temporal evolution of the radiative, electronic and ionic temperature profiles is studied in the presence of a stiff source term. More precisely, the external source terms leads to the separation of the temperature profiles. The relaxation process is then studied. The parameters used for these experiments are summarized in Table 1. The Planck opacities $(\sigma_g)_{g\in[1,G]}$ considered follow the standard Kramers model (see

	Problem 1	Problem 2	Problem 3	Problem 4
c	29.979	29.979	29.979	29.979
a	0.01372	0.01372	0.01372	0.01372
σ_p	$0.5 \cdot T_e^{-2}$	$0.1 \cdot T_e^{-2}$	$0.5 \cdot T_e^{-2}$	$0.1 \cdot T_e^{-2}$
κ	0.1	$0.01379 \cdot (T_e)^{-1/2}$	0.1	$0.01379 \cdot (T_e)^{-1/2}$
$\rho C_{v,i}$	0.15	0.15	0.15	0.15
$\rho C_{v,e}$	0.3	$0.3 \cdot T_e$	0.3	$0.3 \cdot T_e$
T_i	$2.52487 \cdot 10^{-5}$	$2.52487 \cdot 10^{-5}$	$2.52487 \cdot 10^{-1}$	$2.52487 \cdot 10^{-5}$
T_e	$2.52487 \cdot 10^{-5}$	$2.52487 \cdot 10^{-5}$	$2.52487 \cdot 10^{1}$	$2.52487 \cdot 10^{-5}$
T_r	$2.52487 \cdot 10^{-5}$	$2.52487 \cdot 10^{-5}$	$2.52487 \cdot 10^{-1}$	$2.52487 \cdot 10^{-5}$
A	75.19884	15.03978	75.19884	15.03978
Δt	10^{-3}	10^{-3}	10^{-3}	10^{-3}

Table 1: Parameters and initial quantities.

Annex (6.3) and write

$$\sigma_g^P(T_e) = \sigma_P(T_e)\frac{e^{-x_{g-1}} - e^{-x_g}}{b_g}, \qquad x_g = \frac{h\nu_g}{k_b T_e}.$$

Problem 1 and 2. At initial time the three temperatures are set equal. The radiative and electronic source terms are set to zero while a source term is applied on the ionic energy equation and writes

$$Q_i^{n+1/2} = \frac{1}{\Delta t}\int_{t_{n-1}}^{t_n} Q_i dt = \frac{A}{2\Delta t}\left(\mathrm{erf}(\frac{t_n - t_c}{\sqrt{2}}) - \mathrm{erf}(\frac{t_{n-1} - t_c}{\sqrt{2}})\right),$$

where we set $t_c = 10$ and erf is the standard error function

$$\mathrm{erf} : x \mapsto \frac{2}{\sqrt{\pi}}\int_0^x e^{-t^2} dt.$$

See Table 1 for the values of the different parameters used. In addition, all physical units are given in [10] from which these test cases are taken and extended.

Problem 3. The parameters are those of Problem 1 but the initial temperatures are not identical.

Problem 4 This problem is similar to Problem 2 but the ionic energy source term is replaced by a radiative energy source of same value.

In Figure 1 the source function profile Q_i has been displayed in yellow. In Figures 1-3-4-5 the temperature profiles are displayed for different group numbers G for Problem 1 to 4. It is observed that the radiative, electronic and ionic temperatures separate as the source term activates while the temperatures converge toward an equilibrium temperature $T_r = T_e = T_i$ when the source term vanishes. As expected in the case $G = 1$ the results obtained in [8] are correctly recovered. Then as the number of group is increased it is noticed that the temperature relaxation phenomena takes longer. Consequently, for 50 and 100 groups (Figures in bottom left and bottom right), the time interval used has been changed accordingly.

For each problem, the solution profiles are displayed working with 1, 20, 50 and 100 groups. As the number of groups is increased the convergence of the solution profiles is observed. In Figure 2, the numerical solution has been displayed for Problem 1 working with a large time step $\Delta t = 1$. It is observed that the numerical method remains stable even working with a stiff source term. Indeed, even if the characteristic time associated to the source term becomes small comp ared to the time step used, the numerical method behaves efficiently. Similar results have been observed for the other problems.

4.2 $1D$ slab

In this section, numerical results are presented in a 1D setting. The first test case is taken from [12, 30] and consists in a simple $1D$ diffusion problem modeling the evolution of the radiative energies without matter coupling. The numerical results can be compared

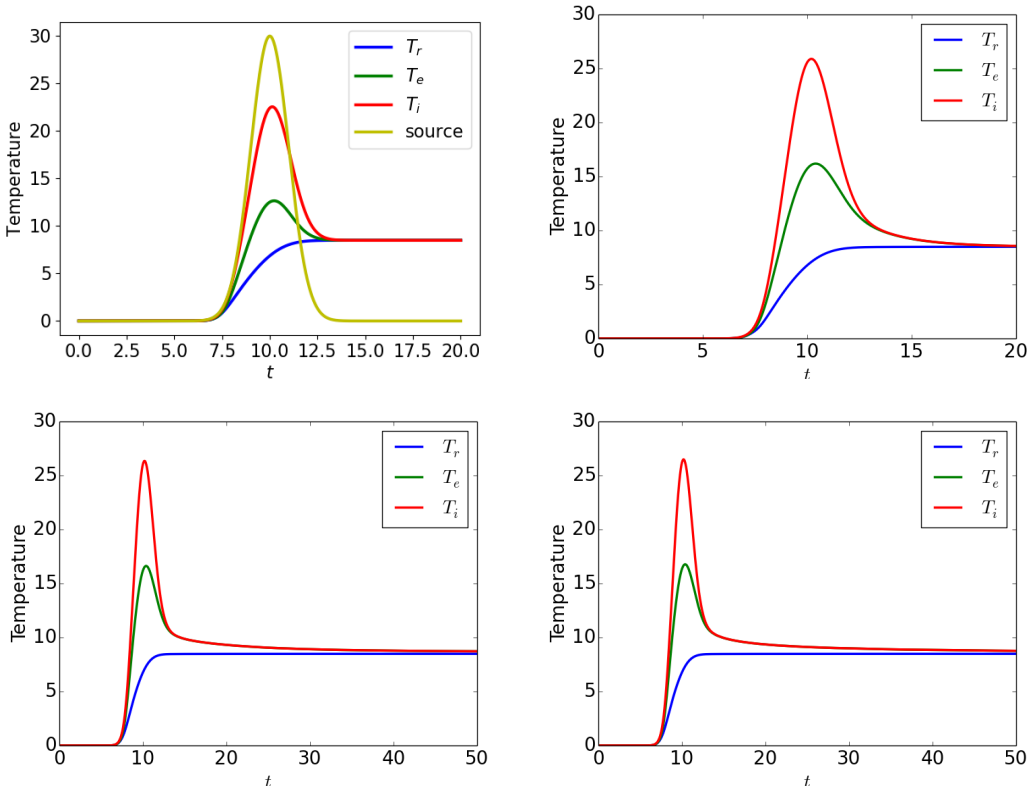

Figure 1: Time evolution of the three temperatures for Problem 1 with 1 (top left), 20 (top right), 50 (bottom left) and 100 (bottom right) groups for $\Delta t = 10^{-3}$.

with analytical references. The second one is also taken from [12, 30], it is a two groups problem for which analytical solutions are also available. The third one is the most challenging and deals with the propagation of a Marshak wave. It was studied in the grey framework in [8] and is now extended to this three temperatures multigroup context.

4.2.1 Multigroup diffusion process

The first test-case performed is taken from [12, 30] and consists in simple $1D$ diffusion problems for which analytical results are available. Here, there is no coupling between radiation and matter and the Rosseland opacity coefficients in the diffusion term are constant in space, they only depend on the group considered and writes

$$\sigma_g^R = 10^{13} \cdot \left(\frac{3.6 \cdot 10^{14}}{\tilde{\nu}_g} \right)^3, \qquad \tilde{\nu}_g = \sqrt{\nu_g \nu_{g-1}}. \tag{28}$$

Here electronic and ionic temperatures are constant and does not evolve in time since the radiation coupling is removed so we only focus on radiation transport. At initial time the radiative temperature is constant in the space domain $[0, L]$ and is denoted T_0.

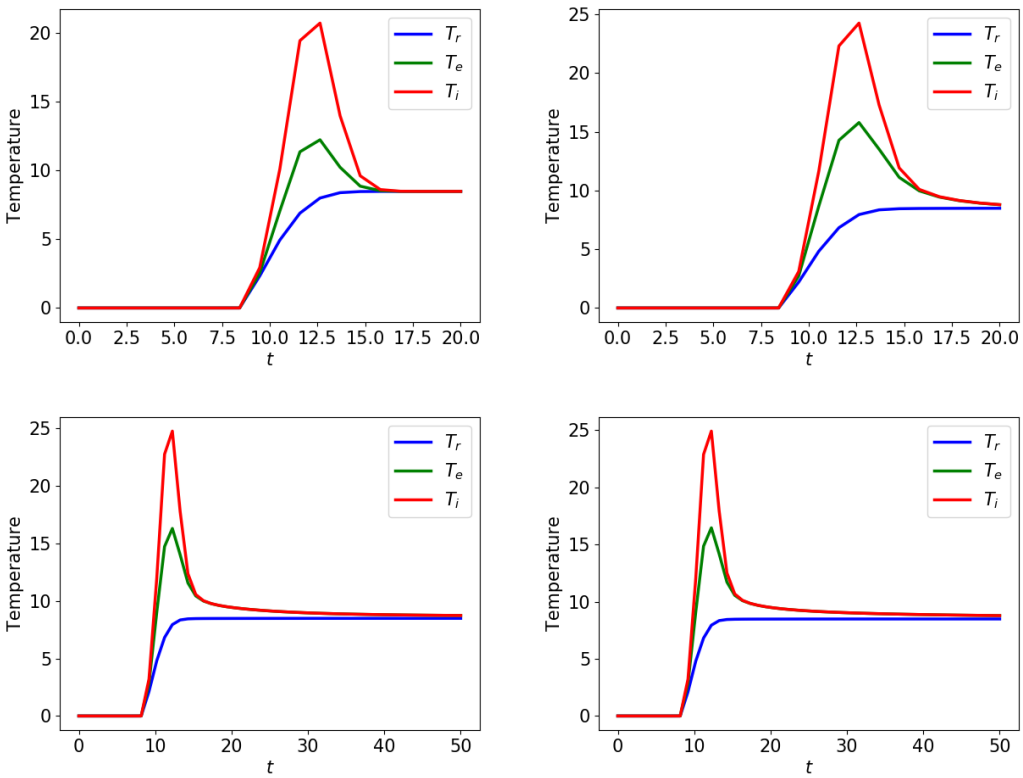

Figure 2: Time evolution of the three temperatures for Problem 1 with 1 (top left), 20 (top right), 50 (bottom left) and 100 (bottom right) groups working with a larger time step $\Delta t = 1$. In the presence of a stiff source term the numerical method remains stable and behaves efficiently.

On the left boundary a radiative energy T_s is enforced and propagates into the domain through diffusion processes. In Table 2 the different parameters used are summarized. The initial radiative energies are initialized as follows

$$\phi_{r,g} = b_g(T_0) a T_0^4, \qquad \forall g \in \{1; ...; G\}\,.$$

A temperature T_s is enforced at the left boundary and the corresponding radiative energies are set as follows

$$\phi_{r,g} = b_g(T_s) a T_s^4.$$

Standard Neumann boundary conditions are enforced on the right boundary. Figure 6 displays the radiative energy associated to each group (the group g is associated to a frequency $\tilde{\nu_g}$ defined in equation (28)) as function of the group frequency in $x = 0.06$ at time $t = 10^{-12}$. The analytical solution is taken from [12] and writes

$$\phi_{r,g} = b_g(T_0) a T_0^4 + \left(b_g(T_s) a T_s^4 - b_g(T_0) a T_0^4 \right) F(\sigma_g, d, t),$$

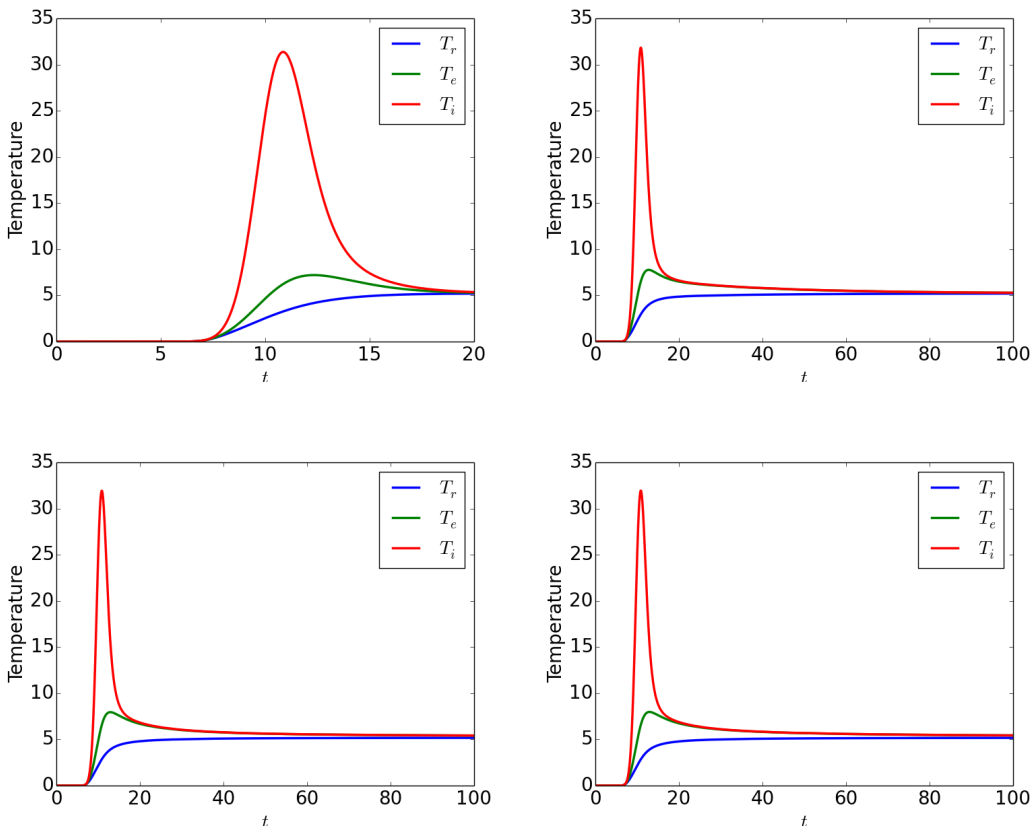

Figure 3: Time evolution of the three temperatures for Problem 2 with 1 (top left), 20 (top right), 50 (bottom left) and 100 (bottom right) groups.

where

$$F(\sigma_g, d, t) = \frac{e^{-\sqrt{3}\sigma_g d}}{2}\left(2 - \mathrm{erf}\left(\frac{1}{4}\sqrt{\frac{3\sigma_g}{ct}}d - \sqrt{ct\sigma_g}\right) - \mathrm{erf}\left(\frac{1}{4}\sqrt{\frac{3\sigma_g}{ct}}d + \sqrt{ct\sigma_g}\right)\right).$$

and we have chosen $d = x = 0.06$ and $t = 10^{-12}$ to plot Figure 6. On Figure 6 it is observed that the numerical solution and the analytical one match perfectly. We considered 60 groups logarithmically spaced in the range $[0.5\text{eV}, 306\text{keV}]$.

c	L	a	T_s	T_0	M	Δt
$2.9979 \cdot 10^{10}$	0.1347368	$1.0267 \cdot 10^{9}$	1500	50	200	10^{-15}

Table 2: Parameters used for the multigroup diffusion test case.

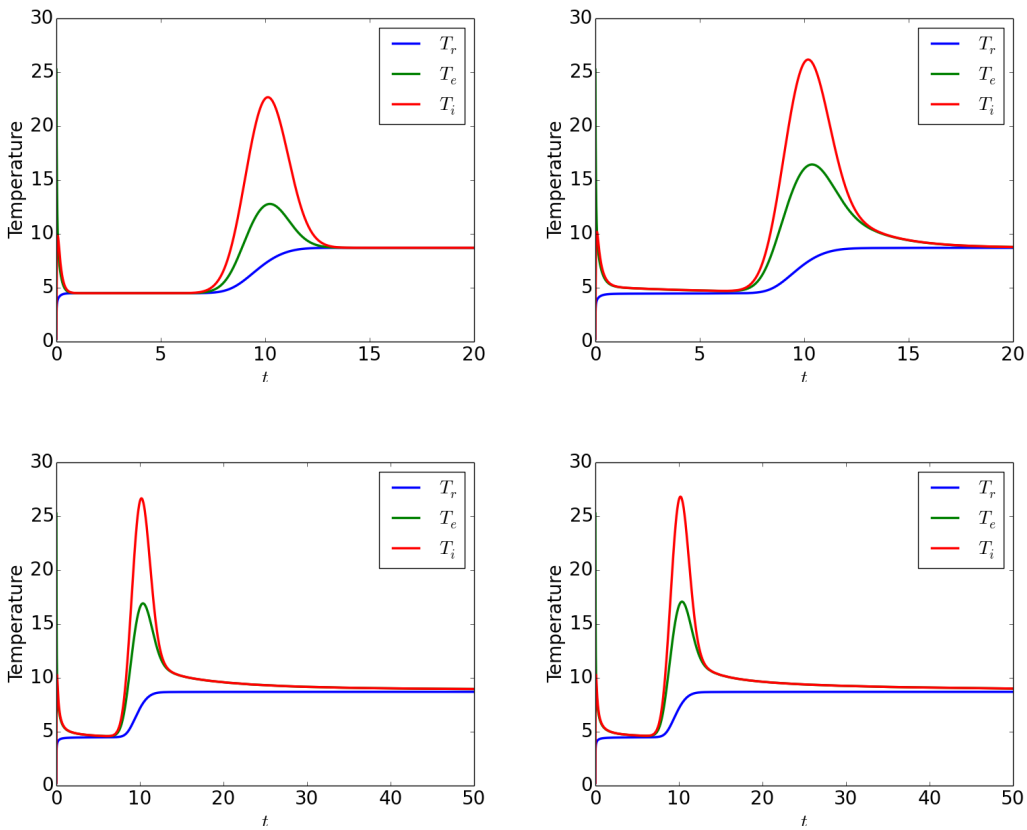

Figure 4: Time evolution of the three temperatures for Problem 3 with 1 (top left), 20 (top right), 50 (bottom left) and 100 (bottom right) groups.

4.2.2 Non-equilibrium radiative transfer with picket fence model

The second test case we consider is also taken from [12, 30]. In [24], analytical solutions for a 1D problem involving non-equilibrium radiative transfer with two radiative energy groups have been developed. Here, radiative energy is injected into the space domain, diffuses, and heats up the gas. The two groups have different opacities so that the radiative energies propagate at different speeds through the medium. The heat capacity is chosen such that $\rho C_{v,e} = \rho C_{v,i} = aT^3$ so it ensures $\beta_e = \beta_i = 1$. The electron-ion coefficient κ is set large enough to prevent an electronic and ionic temperature decoupling so we have $T_e = T_i$. The number of groups is $G = 2$. The opacities $\sigma_g = \sigma_g^R$ and the coefficients b_g are constant in space and are summarized in Table 3. The Planck opacity is defined by $\sigma_P = \sum_g b_g \sigma_g$. No electronic nor ionic source term is enforced but we consider a radiative source term given by

$$Q_{r,g}(t,x) = \begin{cases} c\sigma_P b_g T_s^4 & \text{if } t \leq t_0 \text{ and } x \leq x_0, \\ 0 & \text{otherwise} \end{cases}$$

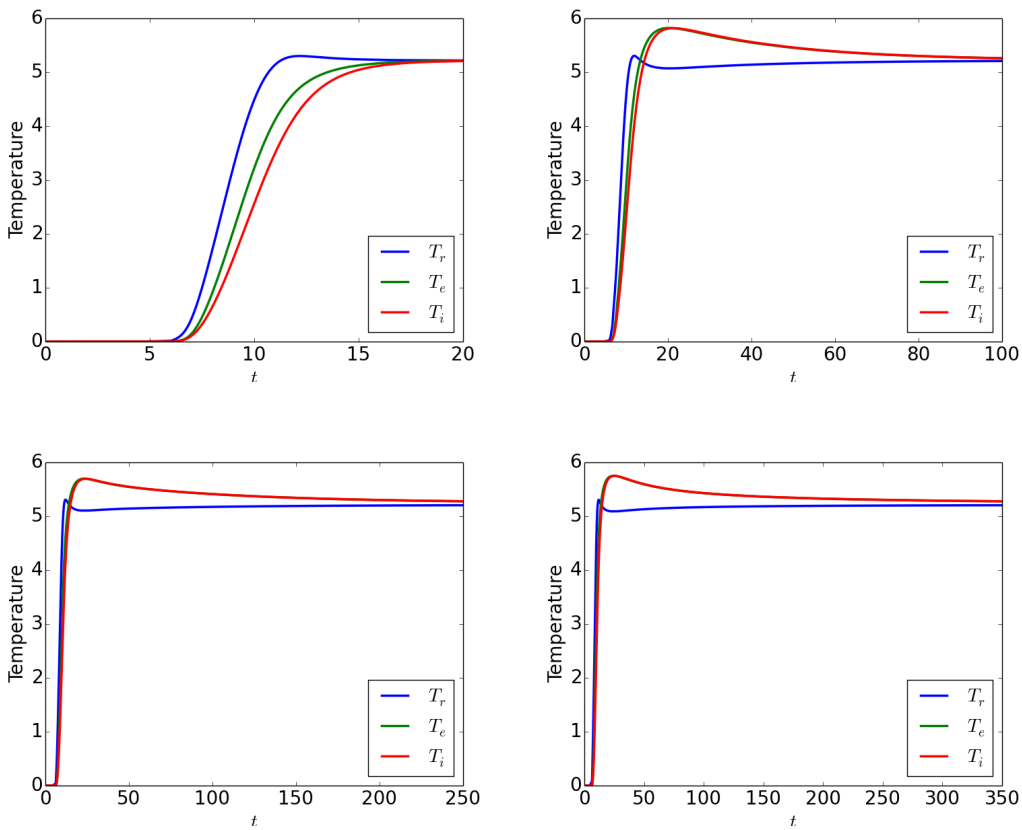

Figure 5: Time evolution of the three temperatures for Problem 4 with 1 (top left), 20 (top right), 50 (bottom left) and 100 (bottom right) groups.

The radiative energies are initially set to

$$\phi_{r,g} = ab_g T_0^4$$

c	L	a	b_g	σ_1	σ_2	T_s	T_0	x_0	t_0	M	Δt
29.979	102.4	$5.670 \cdot 10^{-5}$	1/2	2/101	200/101	1	10^6	1/2	$10/c$	1024	$0.1/c$

Table 3: Parameters for the test case.

Define the following dimensionless energies

$$U_g = \frac{\phi_{r,g}}{aT_s^4}, \quad g = \{1;2\} \qquad V = \frac{\phi_e}{aT_s^4} = \left(\frac{T_e}{T_s}\right)^4.$$

Neumann boundary conditions are enforced on the left boundary while the temperature is fixed to 0 at the right boundary. In Figure 7 the values of U_1, U_2 and V are displayed

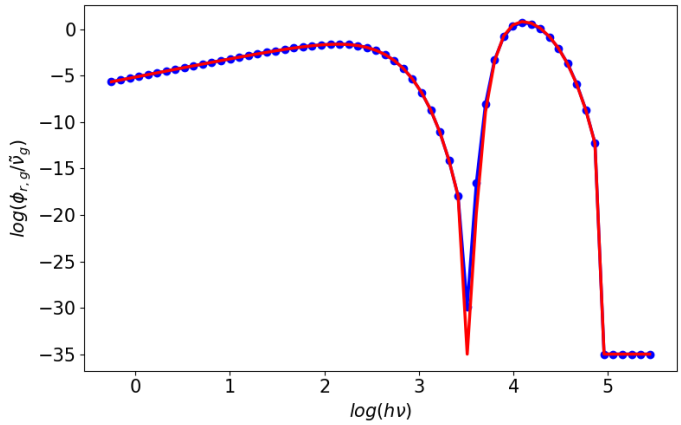

Figure 6: Numerical radiative energy per group at $x = 0.06$ and $t = 10^{-12}$ in blue and analytical solution in red.

at time $t = 3$ and $t = 30$. It is observed that the numerical solutions totally match with the analytical ones.

4.2.3 Propagation of a Marshak wave

The last test case we study consist in the propagation of a Marshak wave. This test case is taken from [8, 26] and extended in this multigroup context. The space interval chosen is $[0, 0.5]$, the temperature at the left boundary is imposed at T_s, meaning that the radiative energies are fixed at

$$\phi_{r,g} = b_g(T_s)aT_s^4.$$

The temperature at the right boundary is fixed at T_0 and thus the radiative energies are

$$\phi_{r,g} = b_g(T_0)aT_0^4.$$

The electron-ion coupling coefficient κ is chosen large enough to ensure $T_e = T_i = T_m$. The initial condition is $T_m = T_r = T_0$ and

$$\phi_{r,g} = b_g(T_0)aT_0^4.$$

The time step used is $\Delta t = 0.001$. In Table 4 the parameters of the simulation are summarized. The Rosseland opacities formulae chosen writes

$$\sigma^R_{g,j+1/2} = \sigma^P_g \left(\frac{T_{e,j} + T_{e,j+1}}{2} \right).$$

In Figure 8 the solutions are displayed for only one group $G = 1$ at time $t = 0.74$

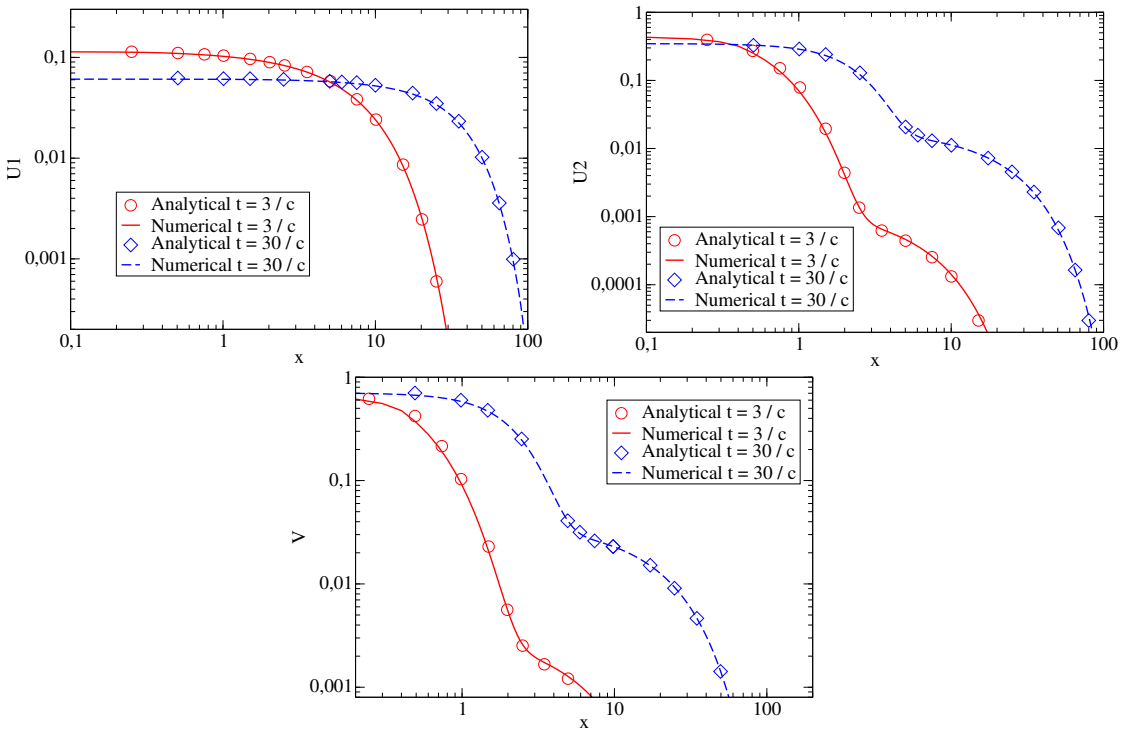

Figure 7: Profiles of U_1 (upper left), V (down) and U_2 (right).

c	L	$\rho C_{v,i}$	$\rho C_{v,e}$	$\sigma_P = \sigma_R$	κ	T_s	T_0
299.79	0.5	0.27	0.03	$300 \cdot T_m^{-3}$	10^{30}	1	10^{-6}

Table 4: Parameters used for the Marshak wave test case.

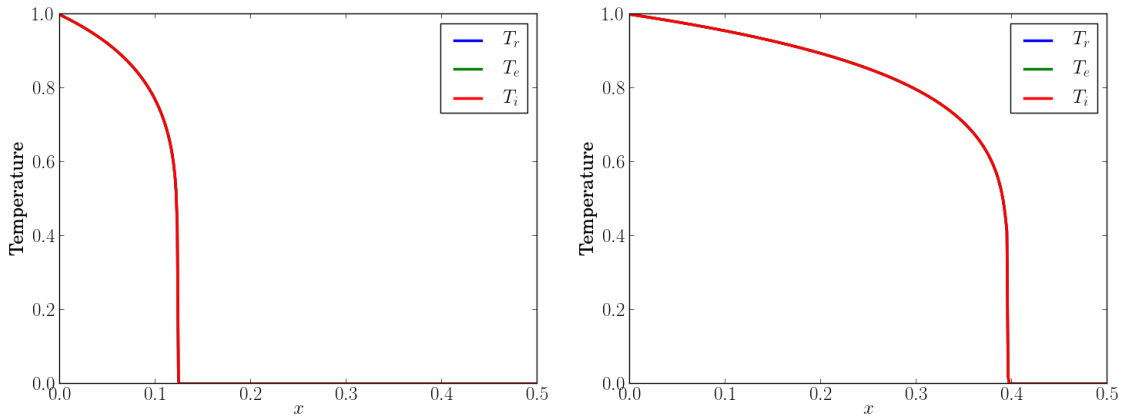

Figure 8: Temperature profiles using 400 cells at time $t = 0.74$ (left) and $t = 7.4$ (right).

and $t = 7.4$. The numerical results displayed correctly match with those obtained in the grey case [8]. Figures 9 displays the multigroup solutions at time $t = 0.074$ using 400 cells using $6, 8, 20$ and 50 groups. A convergence of the solution is observed as the number of group G increases. In addition, it is noticed that the material and radiative temperatures (respectively $T_m = T_i = T_e$ and T_r) tend to separate as the number of groups G increases.

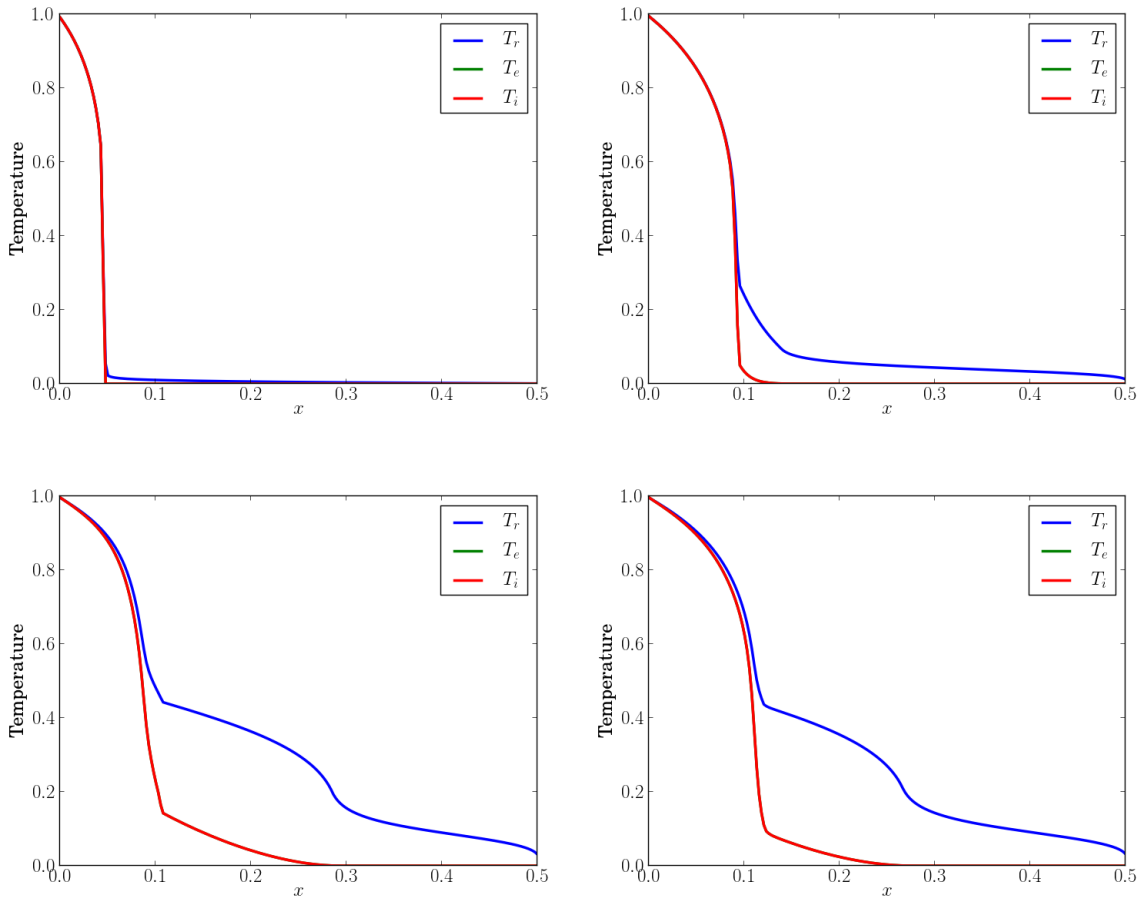

Figure 9: Temperature profiles for 6 groups (left) and 8 groups (right), 20 groups (bottom left) and 50 groups (bottom right) using 400 cells.

5 Conclusion

In the present work, robust and accurate numerical schemes have been proposed and analyzed for solving a multigroup three temperature plasma model in 0D and 1D. The reformulation strategy of [8] extended to this multigroup context leads to the derivation of numerical schemes which are naturally well-suited to handle stiff source terms and can

be analyzed. Indeed, particularly attractive numerical features such as unconditional positivity of the solution, energy conservation or convergence of the algorithm have been proven. We underline that these numerical properties may be difficult to prove while working with this three temperature multigroup model, therefore we believe the methodology presented here is compelling.

More precisely, in the 0D setting a first L^∞ stable scheme has been developed. However, for 1D problems this methodology requires to solve huge systems of size $(G \times M)^2$ and can not be used for a large number of cells or number of groups. Consequently, a variant scheme ensuring the positivity of the discrete solution has been proposed and analyzed. We point out that this strategy naturally extends to multi-dimension problems on unstructured meshes. Another interesting perspective consists in studying the coupling with a full hydrodynamic solver. This will be investigated while keeping the attractive properties obtained in the present work. Of course, the algorithm numerical costs involved in such coupling while studying multi-dimension problems will be a critical issue. Consequently special numerical cares in addition to a careful performance study must be undertaken in order to address it.

6 Appendix

6.1 Initial guess to enhance the convergence speed

Even though the decoupling strategy used enables to greatly reduce the computational times, it is observed that the algorithm is still very slow to reach convergence. Thus, in this section, we propose to speed up the convergence of the algorithm by improving the initial condition of the algorithm. The "natural" initialization would be

$$\phi_{r,g,j}^{n+1,0} = \phi_{r,g,j}^{n} \quad \forall g \in [1, G]; \quad \phi_{e,j}^{n+1,0} = \phi_{e,j}^{n}, \quad \phi_{i,j}^{n+1,0} = \phi_{i,j}^{n}.$$

However, the solution at time t^{n+1} can be significantly different from the solution at time t^n, thus making the convergence of the method very slow. That is why a better initialization (initial guess) is considered for the iterative method is proposed. To do so we first compute an iteration using the grey model ($G = 1$) with the initial conditions

$$\phi_{r,j}^{0} = \sum_{g=1}^{G} \phi_{r,g,j}^{n}, \qquad \phi_{e,j}^{0} = \phi_{e,j}^{n}, \qquad \phi_{i,j}^{0} = \phi_{i,j}^{n}.$$

Denoting $\phi_{r,j}^{grey}, \phi_{e,j}^{grey}, \phi_{i,j}^{grey}$ the results obtained after this "grey" iteration, the initial guest for the multigroup method chosen is

$$\phi_{r,g,j}^{n+1,0} = b_g(T_{e,j}^{grey})\phi_{r,j}^{grey} \quad \forall g \in [1, G], \quad \phi_{e,j}^{n+1,0} = \phi_{e,j}^{grey}, \quad \phi_{i,j}^{n+1,0} = \phi_{i,j}^{grey}.$$

Remark. This prediction is particularly relevant in the diffusion limit $\sigma_P \to +\infty$ because the solutions for the grey model and the multigroup models are equal (if the relaxation and diffusion opacities used for the grey model, respectively σ_g and σ_g^R are

correctly chosen). Table 5 shows the computing times for several values of G and M with and without the "grey" initial guess for the numerical test case described in section 4.2.3 with $\sigma_g^R = \sigma_P$ independent of the group.

G	M	Computing time with prediction (s)	Computing time without prediction (s)
10	400	3300	3900
20	400	2900	3600
30	400	3800	4150
50	200	2650	4250

Table 5: Computing times with and without prediction.

As a conclusion, the prediction allows to speed up the convergence of the iterative method in the diffusion limit. Of course, if the opacity vary significantly in each group the interest in using this "grey" initialization becomes limited and slow convergence issues may arise.

Remark: we use a full diffusion solve over Δt assuming grey and then use the solution as the starting point.

6.2 Acceleration method

When the computation times becomes too large an acceleration procedure may be considered in order to improve the convergence of the iterative methods. The ideas presented here are not originals and are largely inspired from [22, 9]. For clarity, the acceleration method is presented in the case of an infinite electron-ion coupling coefficient κ so that $T_e = T_i$ but it naturally extends to the general case $T_e \neq T_i$. For simplicity, the quantities at sub-iteration k are denoted without exponent (for instance, we write σ_P instead of $\sigma_P^{n+1,k}$). In this case the decoupling procedure leads to

$$\begin{cases} \phi_{r,g,j}^{k'+1} - \phi_{r,g,j}^{n} - \Delta t \left(\lambda_{g,j+1}(\phi_{r,g,j+1}^{k'+1} - \phi_{r,g,j}^{k'+1}) - \lambda_{g,j}(\phi_{r,g,j}^{k'+1} - \phi_{r,g,j-1}^{k'+1}) \right) = \\ \qquad\qquad\qquad\qquad\qquad\qquad\qquad\qquad c\Delta t \sigma_{g,j}(b_{g,j}\phi_{e,j}^{k'} - \phi_{r,g,j}^{k'+1}), \\ \phi_{e,j}^{k'} = \dfrac{1}{1 + c\sigma_{P,j}\Delta t \beta_{e,j}} \left(\phi_{e,j}^{n} + c\Delta t \beta_{e,j} \sum_{g=1}^{G} \sigma_{g,j}\phi_{r,g,j}^{k'} \right) = f\phi_{e,j}^{n} + (1-f) \sum_{g'=1}^{G} \dfrac{\sigma_{g',j}}{\sigma_{P,j}} \phi_{r,g',j}^{k'}, \end{cases}$$

with $f = 1/(1 + c\sigma_{P,j}\Delta t \beta_{e,j})$. The link between the iterative loops denoted by the indexes k and k' will be detailed. Combining the two previous equations leads to

$$\begin{aligned} (1 + c\Delta t \sigma_{g,j})\phi_{r,g,j}^{k'+1} - \Delta t \left(\lambda_{g,j+1}(\phi_{r,g,j+1}^{k'+1} - \phi_{r,g,j}^{k'+1}) - \lambda_{g,j}(\phi_{r,g,j}^{k'+1} - \phi_{r,g,j-1}^{k'+1}) \right) \\ = \phi_{r,g,j}^{n} + c\Delta t \sigma_{g,j} b_{g,j} f \phi_{e,j}^{n} + c\Delta t \sigma_{g,j} b_{g,j}(1-f) \sum_{g'=1}^{G} \frac{\sigma_{g',j}}{\sigma_{P,j}} \phi_{r,g',j}^{k'}. \end{aligned}$$

When $\sigma_{g,j}$ tends to infinite (opaque medium), the iterative process may be arbitrary slow. We give a brief explanation of it. In this situation, the diffusion terms are small

in front of the $c\Delta t\sigma_{g,j}$ term. At the zeroth order, the solution tends to the solution of the equation in infinite medium which reads as

$$(1+c\Delta t\sigma_{g,j})\phi_{r,g,j}^{k'+1} = \phi_{r,g,j}^{n} + c\Delta t\sigma_{g,j}b_{g,j}f\phi_{e,j}^{n} + c\Delta t\sigma_{g,j}b_{g,j}(1-f)\sum_{g'=1}^{G}\frac{\sigma_{g',j}}{\sigma_{P,j}}\phi_{r,g',j}^{k'}.$$

Defining the difference between two iterations $\zeta^{k'+1} = \sum_{g=1}^{G}\sigma_{g,j}\phi_{r,g,j}^{k'+1} - \sum_{g=1}^{G}\sigma_{g,j}\phi_{r,g,j}^{k'}$ then

$$\zeta^{k'+1} = (1-f)\sum_{g=1}^{G}\frac{c\Delta t\sigma_{g,j}}{1+c\Delta t\sigma_{g,j}}\frac{b_{g,j}\sigma_{g,j}}{\sigma_{P,j}}\zeta^{k'},$$

which implies

$$|\zeta^{k'+1}| \leq (1-f)|\zeta^{k'}|,$$

then since $0 < (1-f) < 1$, we conclude that the iterative process converges. When $c\Delta t\sigma_{g,j}$ is large comparing to 1, then f is close to 0 and the factor of reduction of the error $(1-f)\sum_{g=1}^{G}\frac{c\Delta t\sigma_{g,j}}{1+c\Delta t\sigma_{g,j}}\frac{b_{g,j}\sigma_{g,j}}{\sigma_{P,j}}$ is close to 1. In these conditions, the convergence is very slow.

Now we take into account the diffusion term, defining

$$\mathcal{L}(\phi_{r,g,.}^{k'+1}) = -\Delta t\left(\lambda_{g,j+1}(\phi_{r,g,j+1}^{k'+1} - \phi_{r,g,j}^{k'+1}) - \lambda_{g,j}(\phi_{r,g,j}^{k'+1} - \phi_{r,g,j-1}^{k'+1})\right),$$

and denoting $\epsilon_{g,j}^{k'+1} = \phi_{r,g,j}^{k'+1} - \phi_{r,g,j}^{k'+1/2}$ where $\phi_{r,g,j}^{k'+1/2}$ is solution of

$$\begin{aligned}(1+c\Delta t\sigma_{g,j})\phi_{r,g,j}^{k'+1/2} + \mathcal{L}(\phi_{r,g,.}^{k'+1/2}) = \phi_{r,g,j}^{n} + c\Delta t\sigma_{g,j}b_{g,j}f\phi_{e,j}^{n} \\ + c\Delta t\sigma_{g,j}b_{g,j}(1-f)\sum_{g'=1}^{G}\frac{\sigma_{g',j}}{\sigma_{P,j}}\phi_{r,g',j}^{k'}\end{aligned}$$

and $\phi_{r,g,j}^{k'+1}$ solution of

$$\begin{aligned}&(1+c\Delta t\sigma_{g,j})\phi_{r,g,j}^{k'+1} + \mathcal{L}(\phi_{r,g,.}^{k'+1}) = \\ &\qquad \phi_{r,g,j}^{n} + c\Delta t\sigma_{g,j}b_{g,j}f\phi_{e,j}^{n} + c\Delta t\sigma_{g,j}b_{g,j}(1-f)\sum_{g'=1}^{G}\frac{\sigma_{g',j}}{\sigma_{P,j}}\phi_{r,g',j}^{k'+1},\end{aligned}$$

then $\epsilon_{g,j}^{k'+1}$ is solution of

$$\begin{aligned}&(1+c\Delta t\sigma_{g,j})\epsilon_{r,g,j}^{k'+1} + \mathcal{L}(\epsilon_{r,g,.}^{k'+1}) = \\ &\qquad c\Delta t\sigma_{g,j}b_{g,j}(1-f)\sum_{g'=1}^{G}\frac{\sigma_{g',j}}{\sigma_{P,j}}\epsilon_{r,g',j}^{k'+1} + c\Delta t\sigma_{g,j}b_{g,j}(1-f)\sum_{g'=1}^{G}\frac{\sigma_{g',j}}{\sigma_{P,j}}(\phi_{r,g',j}^{k'+1/2} - \phi_{r,g',j}^{k'}).\end{aligned}$$

At this point, the problem is as difficult to solve as the original one since the groups are still coupled in the last equation. But instead of solving it, we solve a grey equation obtained by assuming some known spectrum for $\epsilon_{r,g,j}^{k'+1} = sp_{g,j}\delta W_j^{k'+1}$ then one solves the last equation summed over the groups

$$(1 + c\Delta t(\sigma_j - (1-f))\sum_{g=1}^{G}(\sigma_{g,j}b_{g,j}\sum_{g'=1}^{G}\frac{\sigma_{g',j}}{\sigma_{P,j}}sp_{g',j}))\delta W_j^{k'+1} + \sum_g \mathcal{L}(sp_{g,.}\delta W_.^{k'+1}) =$$
$$\sum_{g=1}^{G}(c\Delta t\sigma_{g,j}b_{g,j}(1-f)\sum_{g'=1}^{G}\frac{\sigma_{g',j}}{\sigma_{P,j}}(\phi_{r,g',j}^{k'+1/2} - \phi_{r,g',j}^{k'})),$$

with $\sigma_j = \sum_g sp_{g,j}\sigma_{g,j}$, which can be rewritten

$$(1 + c\Delta t f\sigma_j)\delta W_j^{k'+1} + \sum_g \mathcal{L}(sp_{g,.}\delta W_.^{k'+1}) = c\Delta t(1-f)\sum_{g'=1}^{G}\sigma_{g',j}(\phi_{r,g',j}^{k'+1/2} - \phi_{r,g',j}^{k'}).$$

Then $\phi_{r,g,j}^{k'+1}$ is finally updated

$$\phi_{r,g,j}^{k'+1} = \phi_{r,g,j}^{k'+1/2} + sp_g\delta W_j^{k'+1}.$$

The overall sub-iteration (iterations k') algorithm is the following

- Start of the sub-iteration process: multigroup step

  Look for $\phi_{r,g,j}^{k'+1/2}$ solution of

  $$(1 + c\Delta t\sigma_{g,j})\phi_{r,g,j}^{k'+1/2} + \mathcal{L}(\phi_{r,g,.}^{k'+1/2}) =$$
  $$\phi_{r,g,j}^{n} + c\Delta t\sigma_{g,j}b_{g,j}f\phi_{e,j}^{n} + c\Delta t\sigma_{g,j}b_{g,j}(1-f)\sum_{g'=1}^{G}\frac{\sigma_{g',j}}{\sigma_{P,j}}\phi_{r,g',j}^{k'}.$$

- Grey step

  Solve the grey equation

  $$(1 + c\Delta t f\sigma_j)\delta W_j^{k'+1} + \sum_g \mathcal{L}(sp_{g,.}\delta W_.^{k'+1}) = c\Delta t(1-f)\sum_{g'=1}^{G}\sigma_{g',j}(\phi_{r,g',j}^{k'+1/2} - \phi_{r,g',j}^{k'}).$$

- Correction

  $$\phi_{r,g,j}^{k'+1} = \phi_{r,g,j}^{k'+1/2} + sp_{g,j}\delta W_j^{k'+1}.$$

test for convergence of $\phi_{r,g,j}^{k'+1}$, if not converged return to the start of the sub-iteration process.

If converged $\phi^{k+1}_{r,g,j} = \phi^{k'+1}_{r,g,j}$ and $\phi^{k+1}_{e,j} = f\phi^n_{e,j} + (1-f)\sum_{g'=1}^{G} \frac{\sigma_{g',j}}{\sigma_{P,j}}\phi^{k+1}_{r,g',j}$. Concerning the choice of $sp_{g,j}$, starting from the equation on the error at the first k' iteration :

$$(1 + c\Delta t\sigma_{g,j})\epsilon^1_{r,g,j} + \mathcal{L}(\epsilon^1_{r,g,.}) = \\ c\Delta t\sigma_{g,j}b_{g,j}(1-f)\sum_{g'=1}^{G}\frac{\sigma_{g',j}}{\sigma_{P,j}}\epsilon^1_{r,g',j} + c\Delta t\sigma_{g,j}b_{g,j}(1-f)\sum_{g'=1}^{G}\frac{\sigma_{g',j}}{\sigma_{P,j}}(\phi^{1/2}_{r,g',j} - \phi^0_{r,g',j}).$$

In an infinite medium, this equation becomes

$$(1 + c\Delta t\sigma_{g,j})\epsilon^1_{r,g,j} = c\Delta t\sigma_{g,j}b_{g,j}(1-f)\left(\sum_{g'=1}^{G}\frac{\sigma_{g',j}}{\sigma_{P,j}}\epsilon^1_{r,g',j} + \sum_{g'=1}^{G}\frac{\sigma_{g',j}}{\sigma_{P,j}}(\phi^{1/2}_{r,g',j} - \phi^0_{r,g',j})\right). \tag{29}$$

Then $\epsilon^1_{r,g,j}$ solution of (29) is found to be proportional to $\frac{\sigma_{g,j}b_g}{1/c\Delta t + \sigma_{g,j}}$, thus $\epsilon^1_{r,g,j} = sp_{g,j}\delta W^1_j$. Substituting this expression into (29) and summing over g, we find that δW^1_j is solution of the grey equation

$$(1 + c\Delta t f\sigma_j)\delta W^1_j = c\Delta t(1-f)\sum_{g'=1}^{G}\sigma_{g',j}(\phi^{1/2}_{r,g',j} - \phi^0_{r,g',j}). \tag{30}$$

Reciprocally, the matrix $m_{g,g'} = \delta^{g'}_g + c\Delta t\sigma_{g,j}(\delta^{g'}_g - b_{g,j}(1-f)\frac{\sigma_{g',j}}{\sigma_{P,j}})$ thanks to $m_{g,g} > 0$, $m_{g,g'} < 0$ for $g \neq g'$ and $\sum_g m_{g,g'} > 0$ with $\delta^{g'}_g$ the Kronecker symbol, is inversible and the solution of (29) exists and is unique. This solution is thus $\epsilon^1_{r,g,j} = sp_{g,j}\delta W^1_j$ where δW^1_j is solution of (30), which implies that $\phi^1_{r,g,j} = \phi^{1/2}_{r,g,j} + sp_{g,j}\delta W^1_j$ verifies

$$(1 + c\Delta t\sigma_{g,j})\phi^1_{r,g,j} = \phi^n_{r,g,j} + c\Delta t\sigma_{g,j}b_{g,j}f\phi^n_{e,j} + c\Delta t\sigma_{g,j}b_{g,j}(1-f)\sum_{g'=1}^{G}\frac{\sigma_{g',j}}{\sigma_{P,j}}\phi^1_{r,g',j}.$$

The sub-iterative (k') process is thus converged in one step after solving the acceleration equation. Then, since in an opaque medium, the solution at the zeroth order is close to the infinite medium solution, we choose the spectrum $sp_{g,j}$ proportional to $\frac{\sigma_{g,j}b_g}{1/c\Delta t + \sigma_{g,j}}$.

6.3 Computation of the opacities

In this section, the practical computation of the opacities $(\sigma^P_g)_{g\in[1,G]}$ is detailed. Recall the standard Kramers spectral opacity model writes

$$\sigma_\nu(\nu, T_e) = K_P\frac{T_e^\gamma}{e^x b(x)}, \qquad \sigma_P(T_e) = \int_0^{+\infty} b_\nu(\nu, T_e)\sigma_\nu(\nu, T_e)d\nu = K_P T_e^\gamma,$$

where K_P and γ are physical constants which are specified for each test case. Hence by definition

$$\sigma_g^P(T_e) = \frac{1}{b_g}\int_{\nu_{g-1}}^{\nu_g} b_\nu(\nu, T_e)\sigma_\nu(\nu, T_e)d\nu = \sigma_P(T_e)\frac{e^{-x_{g-1}} - e^{-x_g}}{b_g}, \qquad \sum_{g=1}^{G}\sigma_g b_g = \sigma_P.$$

Remark. As the function b decreases exponentially, for high frequency groups the coefficients b_g tend to be very small, thus creating a numerical singularity in the computation of σ_g. More precisely the coefficient $(e^{-x_{g-1}} - e^{-x_g})/b_g$ may lead to numerical issues. In order to overcome this numerical difficulty, the following substitution is proposed to counterbalance the exponential decrease. We first write

$$\frac{\sigma_P(T_e)}{\sigma_g^P(T_e)} = \frac{b_g}{e^{-x_{g-1}} - e^{-x_g}} = \int_{x_{g-1}}^{x_g} b(x)e^x\frac{e^{-x}}{e^{-x_{g-1}} - e^{-x_g}}dx, \qquad x = \frac{h\nu}{k_B T}.$$

Now define the change of variable

$$y = \frac{e^{-x_{g-1}} - e^{-x}}{e^{-x_{g-1}} - e^{-x_g}}, \qquad dy = \frac{e^{-x}}{e^{-x_{g-1}} - e^{-x_g}}dx, \qquad x(y) = x_{g-1} - \ln\left(1 - y\left(1 - e^{x_{g-1}-x_g}\right)\right).$$

Therefore, denoting $f(x) = b(x)e^x$ leads

$$\int_{x_{g-1}}^{x_g} b(x)e^x\frac{e^{-x}}{e^{-x_{g-1}} - e^{-x_g}}dx = \int_0^1 f(x(y))dy,$$

which is correctly suitable for numerical computing.

Remark. The previous Remark shows that the evaluation $(\sigma_g(T_e))_{g\in[1,G]}$ may be numerically expensive. In addition, these quantities need to be updated at each sub-iteration. That is why in practice they are computed at the initial time for several given values of the electronic temperature T_e and only interpolated during the simulation.

Acknowledgment. The authors are thankfull to P. Hoch and E. Labourasse for their help and all the interesting discussions on the present subject. The data are available on request from the authors.

References

[1] S. Bolding, J. Hansel, J. Edwards, J. Morel, and R. Lowrie. Second-order discretization in space and time for radiation-hydrodynamics. *Journal of Computational Physics*, 338, 2017.

[2] R. L. Bowers and J. R. Wilson. A numerical model for stellar core collapse calculations. *Astrophysical Journal, Suppl. Ser.*, 50:115–159, 1982.

[3] A. Burrows, T. Young, P. Pinto, R. Eastman, and T. Thompson. A new algorithm for supernova neutrino transport and some applications. *The Astrophysical Journal*, 539(2):865, 2000.

[4] J. Daligault and J. Simoni. Theory of the electron-ion temperature relaxation rate spanning the hot solid metals and plasma phases. *Physical Review E*, 100(4):043201, 2019.

[5] S.W. Davis, J.M. Stone, and Y.F. Jiang. A radiation transfer solver for athena using short characteristics. *The Astrophysical Journal Supplement Series*, 199(1):9, 2012.

[6] A. Decoster. Fluids equations and transport coefficients of plasmas. Modeling of collisions, Series in applied Mathematics (1998), ISBN 2-84299-055-2.

[7] C. Enaux. Personal communication (2019).

[8] C. Enaux, S. Guisset, C. Lasuen, and Q. Ragueneau. Numerical resolution of a three temperature plasma model. *J. Sci. Comput.*, 82, 2020.

[9] T. Evans, K. Clarno, and J. Morel. A transport acceleration scheme for multigroup discrete ordinates with upscattering. *Nuclear Science and Engineering*, 165, 07 2010.

[10] T.M. Evans and J.D. Densmore. Methods for coupling radiation, ion, and electron energies in grey implicit monte carlo. *Journal of Computational Physics*, 225(2):1695–1720, 2007.

[11] J. W. Ferguson, D.R. Alexander, F. Allard, and al. Low-temperature opacities. *The Astrophysical Journal*, 623(1):585–596, 2005.

[12] M. Gonzalez, N. Vaytet, B. Commercon, and J. Masson. Multigroup radiation hydrodynamics with flux-limited diffusion and adaptive mesh refinement. *Astronomy & Astrophysics*, 578:A12, 2015.

[13] H.-T. Janka. Explosion mechanisms of core-collapse supernovae. *Annual Review of Nuclear and Particle Science*, 62:407–451, 2012.

[14] H.-T. Janka, K. Langanke, A. Marek, G. Martinez-Pinedo, and B. Muller. Theory of core-collapse supernovae. *Phys. Rep.*, 442(1-6):38–74, 2007.

[15] E. Larsen, A. Kumar, and J. Morel. Properties of the implicitly time-differenced equations of thermal radiation transport. *Journal of Computational Physics*, 238:82–96, 2013.

[16] E. W. Larsen and B. Mercier. Analysis of a monte carlo method for nonlinear radiative transfer. *Journal of Computational Physics*, 71(1):50 – 64, 1987.

[17] M. Liebendorfer, O.E.B. Messer, A. Mezzacappa, S.W. Bruenn, C.Y. Cardall, and F.K. Thielemann. A finite difference representation of neutrino radiation hydrodynamics in spherically symmetric general relativistic spacetime. *The Astrophysical Journal Supplement Series*, 150(1):263–316, 2004.

[18] B. Mercier. Application of accretive operators theory to the radiative transfer equations. *SIAM Journal on Mathematical Analysis*, 18(2):393–408, 1987.

[19] D. Mihalas and B. Mihalas. Foundations of Radiation Hydrodynamics. Oxford University Press (1984), ISBN 0-19-50347-6.

[20] DS Miller, JR Wilson, and RW Mayle. Convection above the neutrinosphere in type ii supernovae. *The Astrophysical Journal*, 415:278–285, 1993.

[21] J. Morel and R. McClarren. Stability of explicit radiation-material coupling in radiative transfer calculations. *J. Quant. Spectr. Rad. Transf.*, 112:1518–1524, 07 2011.

[22] J.E. Morel, E.W. Larsen, and M.K. Matzen. A synthetic acceleration scheme for radiative diffusion calculations. *Journal of Quantitative Spectroscopy and Radiative Transfer*, 34(3):243 – 261, 1985.

[23] D. Semenov, T. Henning, C. Helling, M. Ilgner, and E. Sedlmayr. Rosseland and planck mean opacities for protoplanetary discs. *A&A*, 410(2):611–621, 2003.

[24] B. Su and G. Olson. Non-grey benchmark results for two temperature non-equilibrium radiative transfer. *Journal of Quantitative Spectroscopy and Radiative Transfer*, 62(3):279–302, 1999.

[25] F.D. Swesty and E.S. Myra. A numerical algorithm for modeling multigroup neutrino-radiation hydrodynamics in two spatial dimensions. *Astrophysical Journal, Supplement Series*, 2009, ApJS, 181, 1:1–52, 2009.

[26] T.J. Urbatsch and T.M. Evans. Milagro Version 2. An implicit Monte Carlo Code for Thermal Radiative Transfer: Capabilities, Development, and Usage. LA-14195-MS (2006).

[27] B. van der Holst, G. Toth, I.V. Sokolov, and al. CRASH: A block adaptive-mesh code for radiative shock hydrodynamics. implementation and verification. *The Astrophysical Journal Supplement Series*, 194(2):23, 2011.

[28] R.B. Williams. 2005, Ph.D. Thesis, Massachusetts Institute of Technology, Dept. of Nuclear Engineering.

[29] A.B. Wollaber, E.W. Larsen, and J.D. Densmore. A discrete maximum principle for the implicit monte carlo equations. *Nuclear Science and Engineering*, 173(3):259–275, 2013.

[30] W. Zhang, L. Howell, A. Almgren, A. Burrows, J. Dolence, and J. Bell. Castro: A new compressible astrophysical solver. multigroup radiation hydrodynamics. *The Astrophysical Journal Supplement Series*, 196(2):20, 2011.